Study of Interface Adhesive Properties of Wurtzite Materials for Carbon Fiber Composites

by

Magdian Ulises Galan Vera

A Dissertation Presented in Partial Fulfillment
of the Requirements for the Degree
Doctor of Philosophy

Approved July 2013 by the
Graduate Supervisory Committee:

Henry Sodano, Chair
Hanqing Jiang
Kiran Solanki
Jay Oswald
Gil Speyer

ARIZONA STATE UNIVERSITY

August 2013

ABSTRACT

Recently, the use of zinc oxide (ZnO) nanowires as an interphase in composite materials has been demonstrated to increase the interfacial shear strength between carbon fiber and an epoxy matrix. In this research work, the strong adhesion between ZnO and carbon fiber is investigated to elucidate the interactions at the interface that result in high interfacial strength. First, molecular dynamics (MD) simulations are performed to calculate the adhesive energy between bare carbon and ZnO. Since the carbon fiber surface has oxygen functional groups, these were modeled and MD simulations showed the preference of ketones to strongly interact with ZnO, however, this was not observed in the case of hydroxyls and carboxylic acid. It was also found that the ketone molecules ability to change orientation facilitated the interactions with the ZnO surface. Experimentally, the atomic force microscope (AFM) was used to measure the adhesive energy between ZnO and carbon through a liftoff test by employing highly oriented pyrolytic graphite (HOPG) substrate and a ZnO covered AFM tip. Oxygen functionalization of the HOPG surface shows the increase of adhesive energy. Additionally, the surface of ZnO was modified to hold a negative charge, which demonstrated an increase in the adhesive energy. This increase in adhesion resulted from increased induction forces given the relatively high polarizability of HOPG and the preservation of the charge on ZnO surface. It was found that the additional negative charge can be preserved on the ZnO surface because there is an energy barrier since carbon and ZnO form a Schottky contact. Other materials with the same ionic properties of ZnO but with higher polarizability also demonstrated good adhesion to carbon. This result substantiates that their induced interaction can be facilitated not only by the

polarizability of carbon but by any of the materials at the interface. The versatility to modify the magnitude of the induced interaction between carbon and an ionic material provides a new route to create interfaces with controlled interfacial strength.

DEDICATION

To my family that has encouraged me during this journey.

ACKNOWLEDGMENTS

I would like to thank my advisor Dr. Henry A. Sodano for his advice during the course of this work, but especially I like to thank him for sharing his passion to discover. I would also like to thank the committee members Dr. Hanqing Jiang, Dr. Kiran Solanki, Dr. Jay Oswald and Dr. Gil Speyer. Finally I would like to thank the ASU-CONACYT fellowship for supporting my graduate studies.

TABLE OF CONTENTS

Page

LIST OF TABLES

Table Page

LIST OF FIGURES

CHAPTER 1

INTRODUCTION

Carbon fiber composites are extensively used in engineering applications where low weight and high strength is required, for example the use of carbon fiber composites in aircraft allows reduced fuel consumption and overall greater efficiency. Carbon fiber composites also find use in infrastructure applications and are applied as jackets on concrete cylinders to increase compressive strength and ductility. Other structural applications include the use of straps to reinforce bridge columns. With the wide range of applications of composite materials, it is important to understand their properties to properly design material systems. This chapter will review the current state of art and provide the motivation for the research presented in this dissertation.

1.1 Introduction to fiber reinforced composite materials

Fiber reinforced composites are widely used as structural materials due to their high specific strength, enabled by the low number of defects in the fibers which permits it to have low weight and high strength. Specifically carbon fibers are often sought as an alternative over metallic materials due to their resistance to stress, creep, corrosion, fatigue and high temperatures. A carbon fiber is composed of amorphous carbon, and some of the atoms at the surface can have intermolecular interactions if they are not covalently bonded. However, most of the carbon fiber's surface will be inert since the majority of the atoms are covalently bonded. In addition, carbon fibers possess other useful properties such as having remarkable electrical and thermal conductivity.

A particular case of carbon reinforced composites are polymer matrix composites. The high strength carbon fibers are used to give strength to the composite and the

polymer matrix serves as the structure producing resistance to stress, corrosion and high temperatures. While composites offer certain advantages over other engineering materials, they are inherently complex to engineer due to the drastic difference in mechanical properties of the fiber and matrix. This problem is further complicated since a composite made from a strong fiber and a well-suited matrix may not necessarily result in a strong material because the fiber-matrix interface is equally important in determining the mechanical performance of the composite [1]. In addition, the full potential of the fibers is not fully utilized in the presence of debonding between the matrix and fiber as shown in Figure 1.1.

Several factors affect the interface, including the chemical composition of the carbon fiber, the type of polymer matrix, and the compatibility between the two materials. Mechanical properties such as strength and toughness of composite materials depend on the properties of the interface between the reinforced fiber and the matrix. In this region the physical and chemical properties of the materials play important roles on transferring the forces between the polymer matrix and the carbon fiber. Fibers or matrix delamination will occur when the local stress exceeds the interfacial strength of the fiber with the matrix. It is well known, that a stress concentration will be formed at an interface between dissimilar materials, and thus the bonding can dictate the ultimate performance and strength of the composite [2].

In an effort to address this issue, many studies have been performed to modify the properties of the carbon fiber surface to enhance bonding; these methods include surface oxidation, roughening and functionalization among others [3]. Other techniques are

based on the inclusion of a secondary material with the aim to increase the surface area of contact and improve load transfer [4-7].

Oxidation treatments modify the chemistry of the fiber surface to enhance the chemical reactivity with particular polymer matrix chosen. These treatments are typically performed through wet chemical reactions, dry oxidation, plasma or atmospheric oxidation to create both polar surfaces and fiber roughness that increase chemical interaction or mechanical interlocking between the fiber and matrix [8-12]. The surface chemistry of carbon fiber has also been modified to create active sites to improve wetting which increases adhesion. Other treatments that do no change the chemical properties of the fiber to improve the interphase strength are done by roughening of the carbon surface, wiskerization [13] and polymer deposition [14,15].

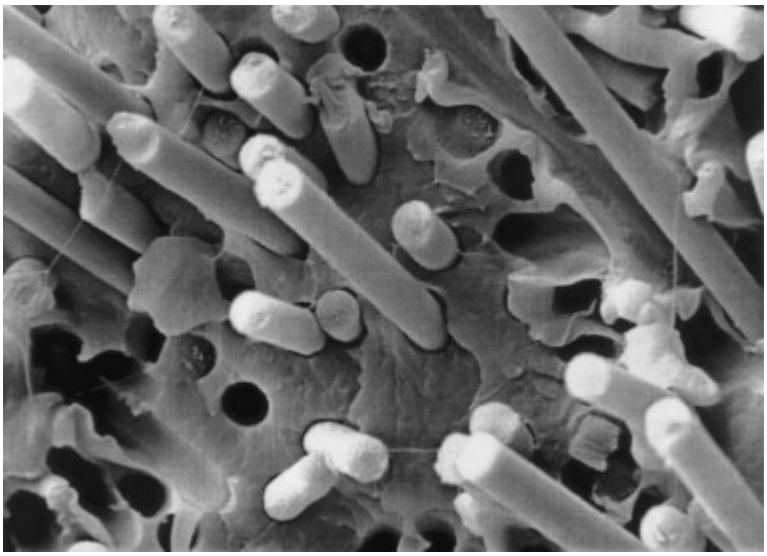

Figure 1.1 Debonding of the fibers from the matrix showing the low adhesion of fibers to matrix that reduces the strength of the composite [16].

The smooth surface and chemical inertness of carbon fibers reduce its ability to create strong bonds with the polymer matrix. The carbon fibers' surfaces are modified by

oxidation, and fiber roughness is increased in order to achieve better mechanical interlocking. When carbon fibers are chemically treated, amorphous carbon present in the outer layer of the fiber are removed by oxidation, which results in a surface with higher roughness that can better carry shear load, leading to stronger interactions with the polymer matrix. With this kind of treatment, the deformed surface of the fiber allows improvement of interface strength.

1.2 Oxidation techniques on carbon fibers

Dry oxidation is performed at elevated temperatures in an environment containing air, oxygen, and carbon dioxide, which creates functional groups on the carbon surface, however the groups are not as stable as those created through chemical treatments. In this process, the surface layer may be burned away unevenly, resulting in a surface with high reactivity. The changes to the surface have detrimental effects due to the reduced fiber tensile strength and modulus.

In wet oxidation (chemical or electrochemical), liquid phase oxidizing agents are used to modify the surface. Variables such as acid concentration, exposure time and temperature affect the results of this process. This treatment causes weight loss and smoothing of the carbon surface, which can reduce the performance of composites. In electrochemical wet oxidation, an electric charge is applied in order to create a more reactive surface to enhance adhesive properties. Although some improvements can be achieved by oxidation, they also damage the fiber's surface in addition to losing tensile strength

1.2.1 Nitric acid oxidation

In the nitric acid oxidation [12] the surface area of the fiber can be increased from the creation of pores in the fiber surface. The pores created by the etching process are visible under the scanning electron microscope (SEM) and help to create mechanical interlocking between the fiber and matrix but also reduce the tensile strength of the fiber. Studies of nitric acid oxidation have shown that amines formed on the carbon fiber create interactions with the epoxy matrix [17]. Thus with this kind of oxidation the interface strength is increased by the physical and chemical properties of the materials at the interface.

Perakslis *et al.* [11] introduced acidic phenolic and carboxyl groups onto carbon fiber surfaces by nitric acid oxidation to increase adhesion with both polyurethanes and epoxy resin matrices. Another study showed that carbon fibers soaked and irradiated in praseodymium nitrate solution had an increase in the fiber surface roughness and oxygen content in functional groups [18]. With this process, the interlaminar shear strength was improved by 13.1% because of a higher content of carboxyl and carbonyl functional groups. Yumitori *et al.* [19] studied the effects of surface treatments for pitch based carbon fibers, with sodium hydroxide (NaOH), sodium bicarbonate ($NaHCO_3$) and sodium carbonate (Na_2CO_3). Interfacial shear strength (IFSS) was increased with an increase in electrical charge up to 1.0×10^{-3} cm^{-2}, suggesting that the oxygen concentration and the amount of hydroxyl and carboxyl groups created a polar surface that increased IFSS. Above 1.0×10^{-3} cm^{-2}, the values of IFSS obtained with NaOH decreased in comparison to the improvement of $NaHCO_3$ and Na_2CO_3. This suggested that NaOH treated fibers had excessive etching on the surface.

1.2.2 Ions irradiation

In this fucntionalization technique molecules, react with the carbon fiber to create new covalent bonds, leaving the surface with a new surface chemistry. This technique is used when a specific surface chemistry is required to match the particular functionally or bonding reaction of the polymer matrix. Since the surface of the carbon fiber is not reduced, the tensile strength of the fiber is not damaged with this process. For example, Park *et al.* used carbon fibers irradiated with Ar^+ ions that changed the chemical properties of the carbon surface and showed that the ion-assisted reaction method resulted in maximum interfacial shear strength of 10.90 MPa for polyacrylonitrile (PAN) carbon fibers with an epoxy matrix [20]. Oxidation reduction and pre-irradiation were studied to investigate the influence on the wetting and the adsorption properties of carbon fibers [21]. It was found that the roughness, surface energy, oxygen content in functional groups and wetting were all increased while the tensile strength was marginally improved for the fibers that were subjected to pre-irradiation, and slightly reduced by the oxidation procedure. Additionally, the interlaminar shear strength was improved by 15% for both oxidation reduction and pre-irradiation treated fibers.

1.2.3 Plasma oxidation

Plasma functionalization is performed under vacuum and high power. In this technique, energy species such as ion, radical and molecules are filled in a vacuum chamber, and the plasma destabilizes the components. When the fibers are introduced into this medium, strong energy interactions occur on the fiber surface which results in the formation of functional groups. This process has been used to oxidize a variety of carbon fibers and it has been shown that the adhesion energy is increased such that the

bonding between the matrix and the fiber improves the strength of the composite [22,23]. With this technique the morphology of the surface is not modified, and the tensile strength of the fiber is not reduced. Since the parameters on this process can be adjusted, several types of fiber functionalization can be obtained, and the variations in the process are mainly affected by type of gas used, time of exposure and power of the plasma equipment. For example as-spun (AS) and high-modulus (HM) fibers were treated with oxygen plasma to form a composite with a poly(1-,4 phenylene-cis-benzobisoxazole) (PBO) epoxy [22]. The untreated PBO composites showed no residue of epoxy while the plasma treated fiber showed large amount of epoxy adhered to the fiber as shown in Figure 1.2. It was found that the surface energy of HM fibers could be increased from 46.2 to 65.7 mJ/m^2 while the tensile strength was negligibly reduced from 5.8 to 5.67 GPa, and the interfacial strength was increased form 32.5 MPa to 44.7 MPa. It was suggested that increases in the cohesive failure led to improved interfacial strength.

Also, Pitch-based P120 carbon fibers were plasma treated, resulting in higher interfacial shear strength when compared to untreated carbon fibers [23]. The load transfer mechanism between the matrix and the untreated fibers was simply frictional, while the increase in oxygen content of the plasma-treated fibers' surface resulted in a greater load transfer because of the increased reactivity of fibers surface.

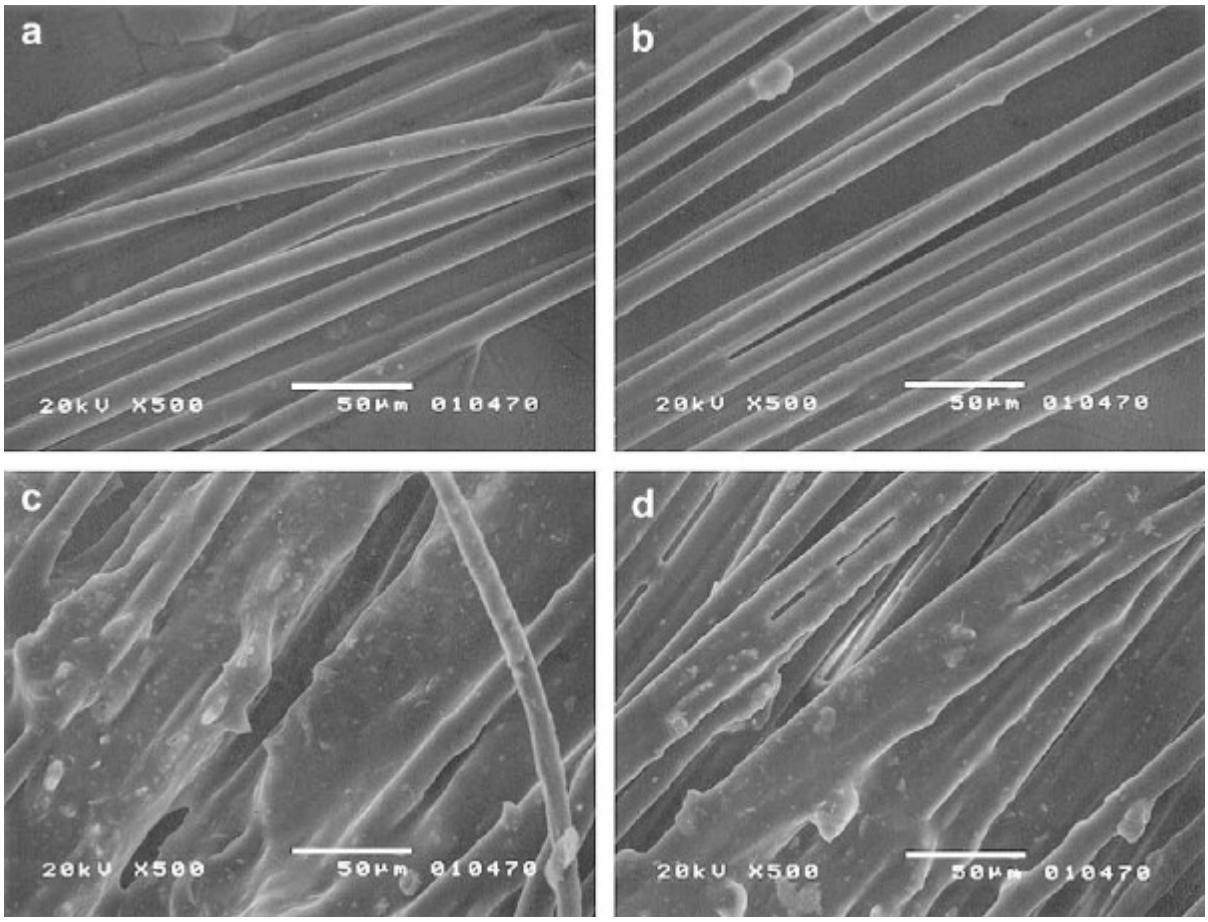

Figure 1.2 SEM images form of fractured epoxy composites from a) untreated AS fibers, b) untreated HM fibers, c) plasma treated AS fibers and d) plasma treated HM fibers [22].

1.2.4 Electrochemical oxidation

The electrochemical oxidation of the fiber has also been used to increase the interactions of carbon fibers by creating pores on the surface that help to increase the mechanical interlocking. In this procedure the porosity of the carbon fiber is increased in order to improve the mechanical interlocking, however, the tensile strength can be damage by the creation of pores [24].

Electrochemical oxidation treatment leads to a higher degree of functionality due to the change of surface morphology and addition of functional groups with high oxygen

content. The process can also lead to unwanted levels of oxidation that are detrimental to the composite's performance. For example Delamar *et al.* [10] employed electrochemical reduction of aryl diazonium on the carbon fibers, which resulted in the increase of 4-nitrophenyl groups on carbon fiber surface leading to an improved adhesion to the epoxy resin. Interfacial shear strength was 63% higher compared to the untreated fibers, although the bonding was dependent on the type of matrix employed which has made it difficult to obtain a universal process for enhancing the interface strength.

Electrochemical treatment of the carbon fibers' surface has been found to reduce carbon fibers' tensile strength while simultaneously increasing the interfacial shear strength due to improved load transfer within the composite. Cao *et al.* [9] observed this with intermittent electrochemical treatment of carbon fiber and phelonic resin as matrix. Treated fibers exhibited significant increases of wettability, and XPS analysis indicated a larger number of oxygenic and nitrogenous functional groups on the surface of the treated fibers. As a result of these chemical and physical changes, the interfacial shear strength was increased by 78%. Szazdi [8] used sodium hydroxide electrolyte and observed an increase of strength. Untreated fibers were tested to 17.3 MPa interfacial shear strength, and the performance was increased to 27.5 MPa with oxidation in NaOH to 44.8 MPa if the fibers were washed.

1.3 Secondary materials as interphase

Unlike oxidative methods where functional groups are added to the surface of the fiber or weak outer layers are removed, non-oxidative treatments involve the deposition of materials such as sizings, whiskers and nanostructures to improve the load transfer and bonding. These non-oxidative treatments can be considered interphase treatments

because a third phase is added to the composite which lies between the reinforcing fibers and the matrix [3]. In this section, several different interphase treatments will be highlighted.

The presence of an interphase surrounding a fiber implies that instead of one interface, there are actually two. For a polymeric sizing layer or polymeric interphase, the strong interaction between the sizing layer and the polymer matrix generally leads to failure at the interphase/fiber interface, which benefits from the enhanced properties of the sizing layer. Sizing layers are typically optimized for adhesion of the sizing layer to the underlying structural fiber. Whisker and nanostructured interphases follow the same analysis; thus rather than a fiber/matrix interface, both the fiber/interphase and interphase/matrix interfaces must be superior to improve the effective composite properties. The whisker/matrix interface is much improved over the sizing/matrix interface because the whiskers interlock with the matrix and have a higher surface area which reduces the stress concentration that inevitably develops.

1.3.1 Sizing on carbon fiber

Fiber sizing is primarily applied to carbon fibers to protect them from damage during handling or weaving. Commercial sizing treatments are also effective in improving the bond between the fiber and matrix. Carbon fibers that do not have surface treatments produce composites with low interlaminar shear strength because of the poor adhesion of the carbon fiber surface with the polymer matrix. Thus, the sizing on the carbon fiber has to be chemically compatible with the polymer and also with the fiber. Paipetis *et al.* [15] found that the sized fiber had higher interfacial shear strength with a small residue of sizing remaining on the fiber and exhibited mixed-mode fracture as shown in Figure 1.3,

while debonding was observed for unsized fibers. Also, the sizing polymers typically increase the acidic groups on the fiber surface which improves wettability and bonding with the matrix, these traits result in higher interlaminar shear strengths.

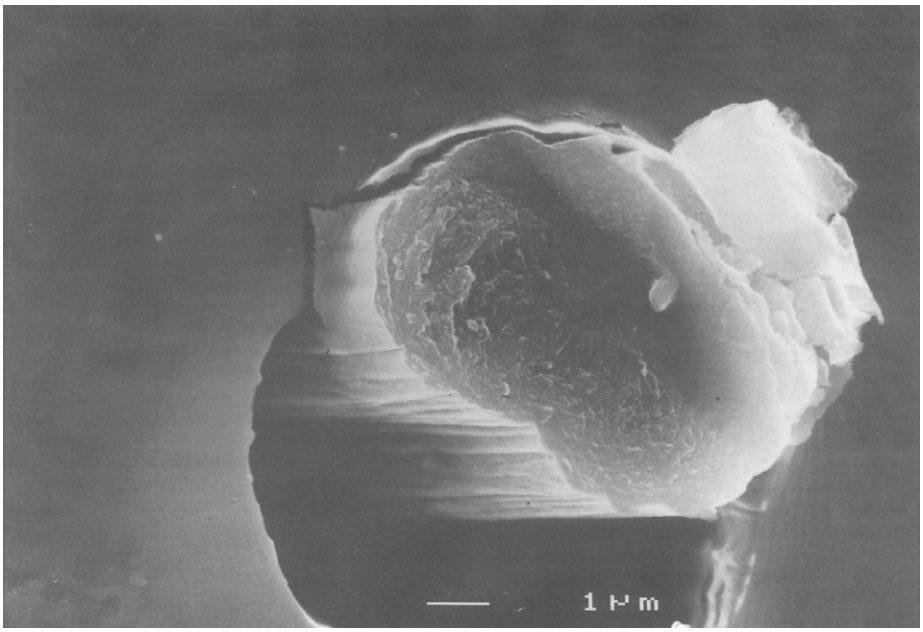

Figure 1.3 SEM image of a fractured surface of sized carbon fiber where the sizing surrounding the fiber shows debonding from the fiber [15].

On a study of sized and unsized fibers it was found that interfacial shear strength for composites with sized fiber was greater than composites with unsized fibers [14]. In addition, the mode of failure was found to be different; for fibers with sizing, the interfacial failure was due to matrix cracking while composites with unsized fibers showed evidence of debonding between the fibers and the matrix. Mader et al. [25] studied both aminopropyltriethoxy silane (APS) and APS with epoxy resin (APS/EP). The sizing promoted high adhesion between the fiber and matrix and provided energy release at the interphase. The release of energy at the interface led to improvement of fatigue resistance of the composite.

Dilsiz *et al.* [26] used Atomic Force Microscopy (AFM) to show the carbon fiber had a modified surface topography with increased roughness caused by the fiber sizing. While the sizing applied to the fiber is often necessary to enhance the durability of the fiber and increase the wetting, the sizing agent is typically suited for only a singular polymer. It is possible to increase the interface strength for certain combinations of sizing and matrix systems, but the same polymer can lead to reduction of strength with a different matrix, which makes difficult to establish a process to universally increase the performance of fiber reinforced composites. The sizing influences the chemical interactions and the mechanical interlocking between the fiber and the epoxy interface. Thus, the flexibility involved in creating tailored interfaces is often limited by the extensive development required to engineer a new sizing to match the polymer matrix. For instance, Yumitori *et al.* [27] found that one particular sizing resin improved interfacial shear strength of polyethersulfone (PES) matrix composite but decreased the shear strength in an epoxy matrix.

1.3.2 Whiskers growth on carbon fibers

An alternative interphase approach is to grow microscale whiskers on the surface of the fiber that protrude into the matrix in order to increase the surface area for bonding and enhance load transfer between fiber and matrix. This process does not rely on chemical reactions or the affinity of the resin to the treatment and therefore the performance is generally independent of the resin system. With this technique it is necessary that the interphase material has high adhesion to the carbon fiber in order to be able to transfer load from the matrix to the fiber.

The whiskerization process involves the nucleation and growth of high strength single crystals such as silicon carbide (SiC) [13] and titanium dioxide (TiO_2) [28] on the fiber surface to obtain higher surface area of contact between the fiber and matrix and increase the mechanical interlocking. The most common method of whiskerization involves the coating of fibers with SiC micro-whiskers through chemical vapor deposition (CVD) processes carried out at temperatures ranging from 1300 °C to 1500 °C. For example, Kowbel *et al.* [13] investigated non-catalytic SiC whisker formations as a method to increase shear and transverse properties of carbon-carbon composites. Whiskers were produced by a silicon oxide (SiO_2) gas reaction with the carbon surface, and different levels of whiskerizations were controlled by adjusting the temperature and time, the whiskers had diameters up to 1um and length up to 10um. Also, a 300% increase of interlaminar shear strength were found with low level of whiskerization; however, the composite's in-plane properties were considerably decreased due to fiber reaction with the precursor materials during high temperature processing. In other words, the carbon fiber served as the source material for the whiskers and this degraded the properties of the fiber. Goan *et al.* [29] synthetized SiC whiskers by CVD at temperatures from 1110 °C to 1700 °C to increase shear strength in carbon fiber composites. In this study, the shear strength increased from 3000 to 10000 psi, but fiber damage was also existent due to the high processing temperatures.

1.3.3 Carbon nanotubes growth on carbon fibers

Carbon nanotubes have also been used as interphase material. The motivation for this material comes from the fact that carbon nanotubes have good mechanical properties, high aspect ratio and surface area. The synthesis of carbon nanotubes is done through

CVD, if the parameters of the CVD growth are controlled properly, the fibers can maintain their tensile strength. However this method is sensitive to small variations in the growth parameters and can drastically reduce the tensile strength as shown in Figure 1.4 [30]. Several studies have been carried out with this material and it was shown that the interface properties can be improved with carbon nanotubes.

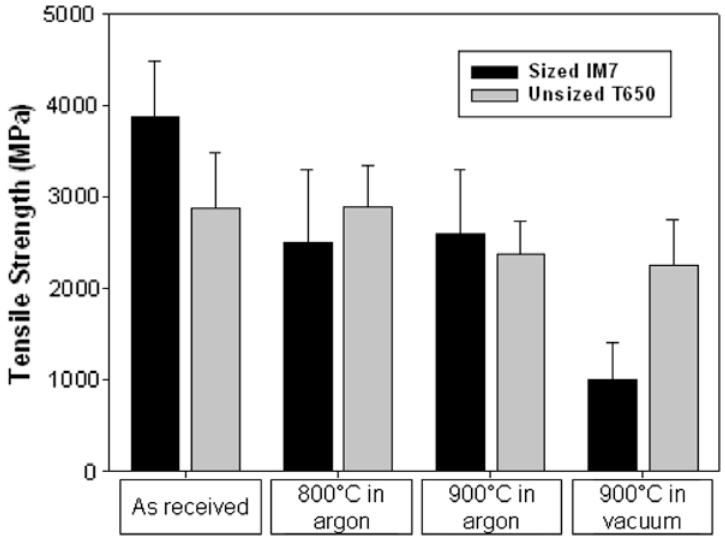

Figure 1.4 Change of carbon fiber tensile strength after synthesis of carbon nanotubes through chemical vapor deposition [30].

In an effort to capitalize upon these properties of carbon nanotubes to reinforce the interface of fiber reinforced composites they were grown on the surface of carbon fibers. Thostenson *et al.* [4] used CVD to grow carbon nanotubes on carbon fibers. Here single fiber fragmentation tests (SFF) showed that the interfacial shear strength of synthesized CNTs on carbon fibers was higher with respect to unsized fibers and catalyst processed fibers, as estimated by the ratio of critical length over diameter ($\boldsymbol{l_c/d}$) in SFF. However tensile testing of fibers was not performed for any set of samples, and thus the reduction of $\boldsymbol{l_c/d}$ could be caused by either improved load transfer from matrix to fiber or the

degradation of fiber's tensile strength. Sager *et al.* [6] employed CVD techniques to grow multi-wall carbon nanotubes (MWCNT) on carbon fibers. The carbon fibers were processed at temperatures up to 900°C for 15 minutes to obtain radially aligned MWCNTs, and 800°C for 30 minutes to produce randomly aligned MWCNTs. They found that the CVD process reduces a fiber's tensile strength by 37% when MWCNT are grown at 900°C, and by 30% when the growth temperature is 800°C. Single fiber fragmentation tests were performed in order to estimate interfacial shear strength, and it was discovered that randomly oriented MWCNTs increased shear strength by 71% while radially oriented MWCNT improved the interfacial shear strength by 11%. The significant increase of shear strength by employing randomly oriented MWCNT suggested that alignment of the MWCNTs with fiber tensile direction improved the load transfer between the MWCNTs and the fiber. Sager [6] also grew multi-wall carbon nanotubes (MWCNT) on carbon fibers through CVD at 900°C for 15 minutes in order to obtain radially aligned MWCNTs and at 800°C for 30 minutes to produce randomly aligned MWCNTs.

Mathur *et al.* [31] synthetized carbon nanotubes by CVD on different fibers: unidirectional (UD), bi directional (BD) and three dimensional (3D). The flexural strength (FS) of the composites were improved by 20% for UD, 75% for 2D and 66% for 3D, while the flexural modulus (FM) were improved by 28%, 54% and 46%, respectively. It was determined that a 5% weight percent increase of carbon nanotubes was enough to improve the mechanical properties. Similarly, Garcia *et al.* [32] synthesized CNTs on the surface of alumina fibers, which led to a 69% increase of interlaminar shear strength. Young *et al.* tested CNT aramid fiber composites, which

caused an 8% increase in impact strength of composite compared to aramid epoxy composites. It suggests that the application of CNTs helped to reduce the crack propagation however this approach is widely accepted to produce greatly reduced fiber strength.

1.4 The ZnO nanowire array as interphase

ZnO nanowires have been extensively investigated for their piezoelectric and semiconductor properties and can be synthetized through several methods, for example CVD [33], vapor-liquid-solid deposition, and aqueous solution based growth methods [34]. ZnO nanowires grow in the (001) direction because the wurtzite structure has polarity in that direction which leads to the preferential deposition on the higher energy facet [35]. However the growth axis and aspect ratio can be controlled by changing the preferential growth direction. For example, in the hydrothermal method the aspect ratio is changed with the inclusion of branched polyethylenimine.

Given the functionality of ZnO nanowires, an alternative whiskerization approach was developed by Lin *et al*. [5] to grow radially aligned ZnO nanowire arrays on the surface of carbon fiber. This process was shown to have certain advantages over CNTs or SiC whiskers due to the low temperature (<90°C) aqueous growth, which allowed the fiber strength to be identically preserved [5,7]. The low temperature processing, does not affect the elastic properties of the fiber and creates a gradient interphase provided by the NWs and a strong interface. In this technique the formation of precipitate has to be prevented because the epoxy has to wet the ZnO nanowires in order to have good load transfer. The hybrid fibers that were synthesized with ZnO nanowires had more than three orders of magnitude increase in surface area and were shown to provide more than a

327% increase in interfacial shear strength compared to the carbon fiber epoxy interface. Lin *et al.* demonstrated the complete infusion of epoxy into ZnO nanowires as shown in Figure 1.5, which provided a better mechanism to transfer load from matrix to fiber [5]. This significant interfacial strength gain combined with the preservation of the composite's in-plane properties provided advances over past whiskerization techniques. The strength enhancement was hypothesized to be due to ZnO's affinity for oxygen groups on the carbon surface. Later, Ehlert *et al.* [36] showed through SFF test that the interfacial shear strength increased with higher concentration of ketones as shown in Figure 1.6. The presence of this group leads to strong adhesion between the nanowires and base fiber as well as enhances load transfer occurring due to mechanical interlocking.

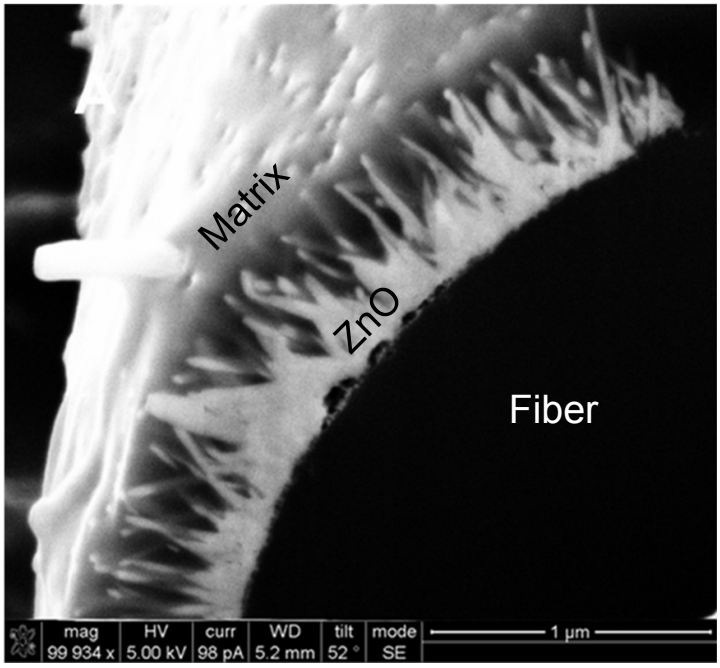

Figure 1.5 Cross section of ZnO nanowires growth on carbon fibers and epoxy wetting on ZnO nanowires [5].

It was also shown that interfacial shear strength increased with the increase of ZnO nanowire length and diameter, and the biggest increase was observed with nanowires of 160 nm diameter. However the interaction between inorganic ZnO and organic carbon fibers has to be studied in more detail in order to understand the nature of the high adhesive energy.

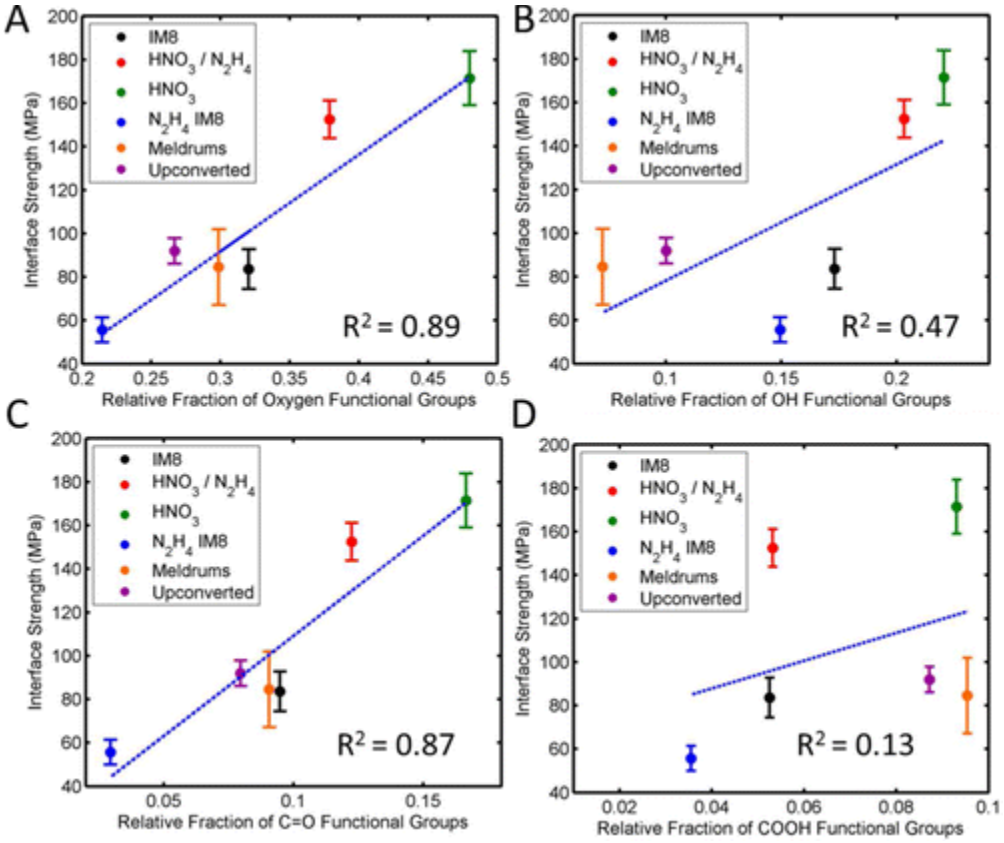

Figure 1.6 Interface shear strength of carbon fibers with ZnO nanowires grown on the surface. The figures shown the correlation of interface strength with a) total oxygen functional groups, b) hydroxyl groups, c) ketones groups and d) carboxylic acid [36].

The previous explanations of interface enhancement like roughness, reduced stress concentration, increased surface area, and interlocking do not apply to the nanowire fiber interface because the area of contact between the ZnO NWs and the fiber is the same area

of contact of the epoxy fiber interphase and the fiber's surface morphology is not modified by the nanowires growth. Thus, intermolecular interactions between the nanowires and the fiber are the most likely explanation for the high adhesive energy and this type of interactions is the subject of this work. In this dissertation the adhesive interaction between the fiber and nanowires will be elucidated through simulations and experimental testing. First it will be shown the calculation of adhesive energy through molecular dynamics simulations and extensive Atomic Force Microscopy (AFM) testing to calculate adhesive energy a variety of different conditions to ultimately provide a method for material selection that produces even greater interfacial strength.

In chapter 2 molecular dynamics (MD) simulations will be used to calculate the adhesive energy between ZnO and carbon surfaces, it will be shown the MD formulation, discuss the properties of ZnO crystalline structure and show how oxygen functional groups on carbon may affect the interface strength. In chapter 3 the AFM liftoff test will be used to measure the adhesive energy between ZnO and several different graphite surfaces, furthermore the liftoff test will show the nature of the intermolecular interactions at the interface and provide insight to the design of interfaces for composite materials.

In chapter 4 ionic materials other than ZnO are studied, ZnS, CdS and CdSe which have the same crystalline structure than ZnO but different lattice parameters producing varying material properties. These materials show a quasilinear relationship between the lattice parameters and other material properties like unite cell volume, elastic constants, polarizability, index of refraction energy gap, etc. In this chapter, the adhesive properties of these materials on carbon will be revealed through AFM liftoff testing to show the

importance of the polarizability for the adhesive energy. Furthermore, CdS nanoparticles will be used on the surface of carbon fiber with subsequent growth of ZnO NWs and single fiber fragmentation testing will be used to calculate the interfacial shear strength and compare the results with the case of ZnO nanoparticles. This testing will lead to a discussion of how induced interactions affect the interface strength and finally, chapter 5 will give the conclusions and recommendation for future work.

CHAPTER 2

MOLECULAR DYNAMICS SIMULATIONS

The properties exhibited by nanocomposites are governed by the constituent phases and the interfacial interactions between these constituents. The mechanical properties of the individual constituents are usually known, but those at the interface are difficult to assess. For example, the mechanics of adhesion between two solids is an important physical process with implications in many technological fields. When two distinct solid surfaces approach, atomic forces and surface energies define the macroscopic properties of the interface.

For this reason it is important to study the properties of the interface in detail. By looking at the two interfaces created by the inclusion of NWs, it can be seen that the surface area of the interface at the NWs and matrix is significantly larger than the area of the ZnO and fiber interface. For this reason, the adhesive properties of the ZnO and carbon interface are critical to the overall properties of the composite. Many approaches exist to model adhesive forces. For example, computational models have been used to elucidate the interactions of interphases, the interface behavior is governed by atomistic interactions and therefore molecular structure has to be taken into account. *Ab initio* calculations have been used to characterize the interface between magnesium oxide (MgO) and silver (Ag) [37], silicon carbide (SiC) (001) and aluminum (Al) [38] as well as α-aluminum oxide (Al_2O_3) (0001) and copper (Cu) (111) [39]. On the other hand, Molecular Dynamics (MD) simulations have also been employed to investigate the mechanical properties of materials and interfaces at the atomic scale with models larger than those *Ab initio calculations*, such as the interface energy between Al and SiC [40].

These types of studies have been useful for gaining a better understanding of the mechanics of separation between two solids. Hence, molecular dynamics simulations have been employed in this dissertation to study the interface behavior of ZnO and carbon with primary attention given to the adhesive energy.

MD simulates the atomic interactions that govern the energetics and properties of a material by describing these interactions with a force field and assuming that atoms are single points with a defined mass [41]. By applying the laws of classical mechanics on the atomic system a range of material properties such as adhesion, diffusion, cracking, creep, etc can be studied [42-44], thus MD provides a tool to study systems at an atomic level. The attractive and repulsive forces that arise at the atomic scale are defined by a force field and can be divided into bonded and non-bonded interactions for neutral systems, while ionic interactions are accounted for by the summation of the electrostatic energies.

2.1 Force field

Force fields are used to relate the energy of a molecule or system of atoms to its geometry by using a set of parameters and an analytical function. It is assumed that these parameters can be determined from experimental data. Various interatomic potentials have been used to describe the interactions between atoms. The Lenard Jones (LJ) potential is an empirical model for Van der Waals forces and describes the attractive or repulsive forces between non bonded atoms. The expression for the potential energy is as follows:

$$u(r) = 4\epsilon\left[\left(\frac{\sigma}{r}\right)^{12} - \left(\frac{\sigma}{r}\right)^{6}\right], \tag{2.1}$$

where ε is the depth parameter and σ is the scale parameter that determines the position of the potential minimum. Based on this potential the force between two atoms can be computed by:

$$F = \frac{dw}{dr} = 24\epsilon\left[\frac{\sigma^6}{r^7} - \frac{2\sigma^{12}}{r^{13}}\right]. \tag{2.2}$$

The positive and negative forces are attractive and repulsive forces respectively, and the equilibrium separation between two atoms is the separation when the net interatomic energy is the minimum as seen in Figure 2.1.

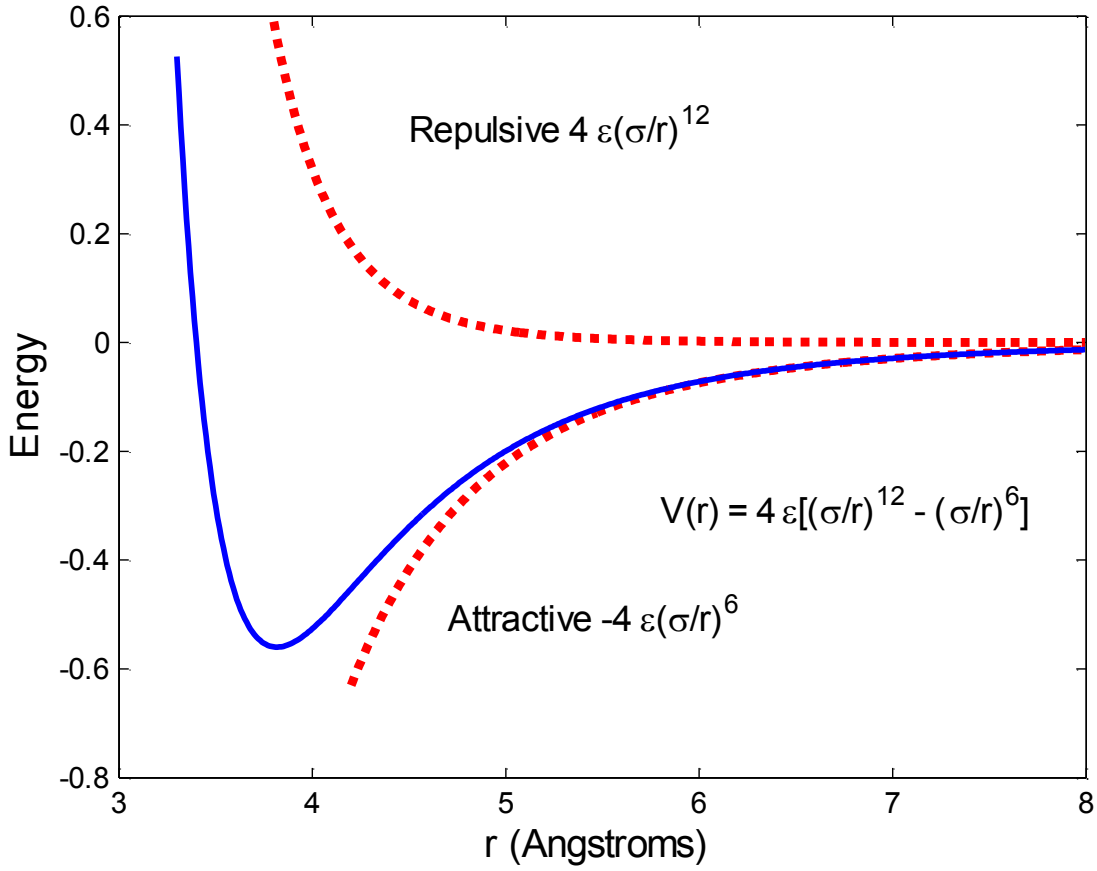

Figure 2.1. Lennard Jones Potential to describe the intermolecular interaction between two atoms.

A Buckingham potential is a two body semi empirical potential that consists of an exponential term to describe the repulsive force between atoms and an r^6 term to describe the attractive force. The Buckingham potential has the form

$$U_r = Ae^{-r/\rho} - \frac{C}{r^6} \tag{2.3}$$

The parameters A, ρ, and C are used to match the potential function respect to the distance r, these parameters are chosen such that material's properties such as lattice and elastic constants are properly characterized.

Covalent bonds in an atomic system can also be modeled by using an analytical function with the potential energy representing the energy of the bond in the equilibrium. For the modeling of a carbon surface, the optimized potential for liquid simulations all atom (OPLS AA) force field can describe the interactions of the covalent bonds and reproduce the properties of carbon. The OPLS potential accounts for the same amount of energy for contraction and expansion, and the empirical parameters represent the equilibrium bond distance, angle and dihedrals. Since the energy calculation can be wrong when the distance between atoms is far from the equilibrium point, it is important to know if the system is close to the equilibrium position prior to performing the MD simulations.

The harmonic potential is used to describe covalent bonding, thus it is assumed that the bonds never break during the simulation, the equations are defined as follows:

$$V_{total} = \sum_{bonds} K_r\left(r - r_{eq}\right)^2 + \sum_{angles} K_\theta\left(\theta - \theta_{eq}\right)^2 + \sum_{dihedrals} \frac{K_n}{2}\left(1 + cos(n\phi - \gamma)\right) + \sum_{i<j}\left(\frac{A_{ij}}{R_{ij}^{12}} - \frac{B_{ij}}{R_{ij}^{6}} + \frac{q_i q_j}{\epsilon_0 R_{ij}}\right), \tag{2.4}$$

where

$$A_{ij} = 4\epsilon_{ij}\sigma_{ij}^{12}$$

$$B_{ij} = 4\epsilon_{ij}\sigma_{ij}^{6} \quad (2.5)$$

and ε is the depth parameter, σ is the size parameter, K is the energy parameter, and r is the distance between only the atoms that are attached by covalent bonds. θ is the angle between three atoms connected by covalent bonds and γ is the coefficient of the torsional angles which is formed between two planes. Lastly, Φ is the angle between two planes that are formed by three atoms connected by covalent bonds.

2.2 Canonical ensembles

An important aspect of molecular dynamics is the thermodynamic ensembles. The ensembles provide a framework to calculate macroscopic properties of a bulk material represented as a system of atoms. These ensembles can consider different conditions such as: particles, volume and energy (NVE); particles, volume and temperature (NVT) [45,46]; and particles, pressure and temperature (NPT) [47]. In a MD simulation the number of particles is given as an input, the volume can be determined by the size of the simulation box, the energy is known from the force field that defines the intramolecular and intermolecular interaction between particles, and the temperature is defined with the following equation:

$$\frac{1}{2}m\langle c_i^2\rangle = \frac{1}{N_f}\sum_{i=1\ldots N_f}\left(\frac{1}{2}m\overline{v}_i^2\right) = \frac{1}{2}k_BT \quad (2.6)$$

where N_f is the total number of degrees of freedom, k_B s the Boltzmann constant, and T is the temperature.

In the NVE microcanonical ensemble, the pressure and temperature are not controlled during the simulation. The main objective is to conserve the energy; however, this may cause the pressure or temperature to overshoot during the time integration process. For this reason this ensemble is only used in systems with high stability and that are thermodynamically insulated from the environment.

In the NVT ensemble, there is a heat bath that is coupled to the system of atoms; thus, the energy of the simulated system can change while the energy of the composite system (simulated system-heat bath) is conserved. The Nose-Hover algorithm can set a system to a specific temperature during a simulation which couples the atomic systems with a heat bath by transferring heat between the bath and the system of atoms in order to keep a desired temperature. The Nose-Hover thermostat is defined from the Newton equations of motion; and they include an additional term that is related to the heat bath. In the equation below there is a free parameter that represents the strength of coupling between the system and the thermostat. This parameter has units of time and is referred to as the relaxation time. Because of this parameter, the algorithm leads to temperature oscillations.

$$\overline{a}_i(t) = \frac{\overline{F}_i(t)}{m_i} - \zeta(t)\overline{v}_i(t) \tag{2.7}$$

the friction coefficient is defined as

$$\frac{d}{dt}\zeta(t) = \frac{N_F}{Q}(k_B T(t) - k_B T_o), \tag{2.8}$$

where the number of degrees of freedom, N_f, is equal to 3N + 1, N is the number of atoms in the system, $T(t)$ is the instantaneous temperature, T_o is the heat bath temperature and k_B is the Boltzman constant. The friction mass parameter Q determines the heat transfer rate

and does not have any significant effects on the system unless the value is fairly large or small. A large value of Q is equivalent to decoupling between the system and the heat bath. If Q is too small the heat is transferred too fast and the algorithm cannot provide a steady temperature.

Unlike the NVP ensemble, the NPT canonical ensemble allows control over both temperature and pressure. The volume of the simulation box is allowed to change and in consequence the pressure of the system can be adjusted. Here, the volume and pressure are inversely related by

$$\kappa = -\frac{1}{V}\left(\frac{\partial V}{\partial P}\right)_T . \tag{2.9}$$

The pressure is controlled by both scaling the volume and using a pressure bath P_{bath}. The volume of the simulation box is scaled by λ which in turn scales the position of the atoms and is mathematically expressed as

$$\underline{\lambda} = 1 - \kappa \frac{\Delta t}{\tau_P}(P - P_{bath})$$

$$r_i^{new} = \underline{\lambda}^{1/3} r_i^{old}, \tag{2.10}$$

where τ_p is the relaxation constant. The size of the simulation box can be changed simultaneously in each direction which is equivalent to isotropic deformation or independently which is equivalent to anisotropic deformation.

2.3 Ionic compounds

Solid ionic compounds consist of stacked, charged atomic layers where the bonding energy consists of attractive and repulsive forces in addition to electrostatic energy. ZnO is a binary compound that can be either zincblend or hexagonal wurtzite structure where each anion is surrounded by four cations at the corners of the tetrahedron and it belongs

to the space group $P_{63}mc$. The wurtzite structure is the most stable and it has a hexagonal unit cell with two lattice parameters *a* and *c*, in the ideal structure, the ratio of these two parameters is equal to 1.633. For wurtzite ZnO, the lattice constants at ambient temperature and pressure conditions are 3.24 and 5.20, the *c/a* and *u* parameters are 1.59 and 0.38 respectively, and the deviation from the ideal wurtzite structure is caused by the ionicity of the material. A schematic representation of the wurtzite structure is shown in Figure 2.2. The structure is composed of two hexagonal closed packed (hcp) sublattices, each of which consists of one type of atom displaced with respect to each other along the c axis by the amount of 3/8 (of the ideal wurtzite structure). Each sublattice consists of four atoms per unit cell where the structure has triangular-arranged, alternating biatomic planes. Because the structure does not have an inversion symmetry, the crystal exhibits polarity in the (0001) and $(000\bar{1})$ surfaces.

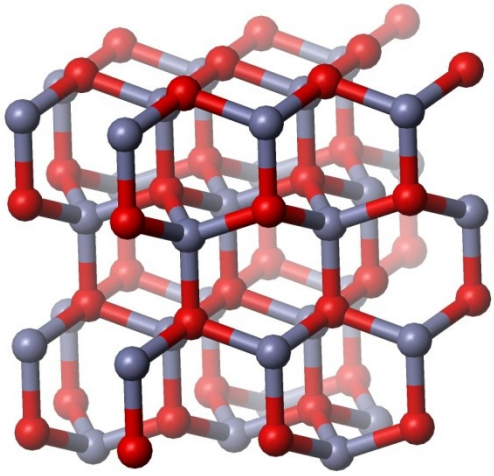

Figure 2.2. Wurtzite Structure

The polar surfaces are Tasker type III [35] that are terminated with Zn (0001) or O $(000\bar{1})$ atoms at the surface. The structure generates an electrostatic field perpendicular to the surface, and the accumulation of electrostatic energy causes the surface energy to

diverge causing instability of the structure which is then energetically compensated by a reconstruction mechanism. Proposed by Tasker [35], the first model of stabilization of the free surfaces is achieved by removal of ¼ of the Zn atoms on the (0001) surface [48]. Recently, another way of stabilization was shown by scanning tunneling microscopy (SMT) and density functional theory (DFT) [49]. In those studies, the surface is stabilized by the spontaneous formation of a high concentration of Zn-deficient triangular pits and step edges terminated by under coordinated oxygen atoms. The formation of these pits is caused by electrostatics that removes the dipole created on the structure. Also the stability of the polar surfaces has been observed with diffraction techniques [50]. As discussed in the literature [6-9], these surfaces are important for their structural characteristics since many material properties depend on the polarity like growth, etching, defect generation, plasticity, polarization, piezoelectricity and adhesion.

2.4 Electrostatic forces

The structure of an ionic compound is held together by the electrostatic forces between the anions and cations, and the force between them is expressed with Coulomb's law, and it is written as follows:

$$\boldsymbol{F}_{ij} = \frac{1}{4\pi\epsilon_0}\frac{q_i q_j}{r_{ij}^2}\hat{\boldsymbol{r}}_{ij} \tag{2.11}$$

where q_i and q_j are the charges of the atoms, the vacuum permittivity is ε_0, and the distance between the two particles is r.

In MD, the Ewald method is used to take into account of the long range electrostatic interactions of periodic systems. The computations are performed in K space, in other words, the atoms are defined in terms of momentum and frequency instead of position and time, and the cutoff of the system is infinity because the long range potential (such as

electrostatic and gravity) decays slower than r^{-d}. Thus, a cutoff is not possible for long range potentials, since this will be equivalent to the introduction of a charged sphere around the particle which is a different phenomenon. This means that each individual charge in the systems interacts with all the charges of the periodic domain. Under periodic conditions, the electrostatic potential of a point r_i for the N number of atoms in the system is obtained by adding the coulomb potential over all the atoms.

2.5 Atomistic stress calculation

The boundaries of the system of atoms can be defined as periodic or non-periodic. Periodic boundary conditions eliminate the effect of the free surface and treats systems with a small number of particles in such a way that the atoms behave like in a bulk material. In periodic boundary conditions, the simulation box is artificially replicated. In other words, when an atom leaves the simulation box, it enters it again from the opposite wall. However, in non periodic boundary conditions, there is no replication of the simulation box, thus forces and in consequence stress is dependent on the conditions at the boundary.

The calculation of stress in molecular dynamics is done through the calculation of the virial stress, and it has been shown that for atomistic calculation, the virial stress is equivalent to the Cauchy stress [51]. The virial stress must be averaged both in time and space in order for these to be equivalent [52]. Recently, it has been suggested that the virial stress is not equivalent to the Cauchy stress [53], but Zumayanan et al [52] have shown that indeed the virial stress is equivalent to the Cauchy stress as long as the correct spatial and temporal averages are taken in the Eulerian reference frame.

The total energy of a system and the position of the atoms are used to calculate the stress tensor per atom, in other words, from the interatomic potential and the position of the atoms the forces acting on a given atom are calculated, and from these forces the virial stress is calculated as follows:

$$\sigma_{ij}^{\alpha} = -\frac{1}{Vol^{\alpha}}\left(m^{\alpha}v_i^{\alpha}v_j^{\beta} + \sum_{\beta,\beta\neq\alpha} r_j^{\alpha\beta} f_i^{\alpha\beta}\right) \tag{2.12}$$

where Vol^{α} is the volume of the atom α, m^{α} is the mass of the atom α, v_i and v_j are the velocities of the α^{th} atom in i direction and j direction respectively, r is the distance between the α and β atoms, and f is the force between the α and β atoms. This quantity is summed over all atoms and divided by the volume of the unit cell in order to obtain the average stress in the unit cell.

The stress on the system can be controlled with a bath coupled to the system. Here the stress tensor is used to change the size of the simulation box, as the volume of the box changes the difference between the internal and external pressure is computed, and it is used to keep adjusting the size of the simulation box to obtain a desired pressure. The volume change of an isotropic system can be written as:

$$\frac{d\eta(t)}{dt} = \frac{1}{Nk_BT_{ext}\tau_p^2}V(t)(P - P_{ext}) \tag{2.13}$$

where N is the total number of atoms, k_B is the Boltzmann constant, $V(t)$ is the volume of the system, P_{ext} is the external pressure, P is the internal pressure, η(t) is an additional degree of freedom, and τ_p is the time parameter for pressure control. Thus, in MD the external pressure (P_{ext}) and the virial stress (P) are equivalent quantities.

2.6 LAMMPS

LAMMPS stands for large scale atomic/molecular massively parallel simulator and will be used for the simulations performed in this dissertation. It is written in C++ and is an open source code distributed under the GNU public license. LAMMPS can be used for a wide range of materials with a variety of force fields and different boundary conditions. The LAMMPS code is parallelized using Message Passing Interface (MPI) and uses spatial decomposition, so a number of atoms in the physical domain are assigned to each processor.

In LAMMPS, the equations of motion are solved numerically and an integration method is necessary. Here, the velocity Verlet algorithm is used to determine the position and velocity of the atoms at every time step and is represented by the following equations:

$$r(t+\Delta t) = r(t) + v(t)\Delta(t) + \frac{1}{2}a(t)\Delta t^2 + \frac{1}{6}b(t)\Delta t^3 + O(\Delta t^4)$$

$$r(t-\Delta t) = r(t) - v(t)\Delta(t) + \tfrac{1}{2}a(t)\Delta t^2 - \tfrac{1}{6}b(t)\Delta t^3 + O(\Delta t^4) \qquad (2.14)$$

Adding these equations:

$$r(t+\Delta t) = 2r(t) - r(t-\Delta t) + a(t)\Delta t^2 + O(\Delta t^4)$$

$$r(t+\Delta t) = r(t) + v(t)\Delta t + \frac{1}{2}a(t)(\Delta t)^2$$

$$v(t+\Delta t) = v(t) + \tfrac{a(t)+a(t+\Delta t)}{2}a(t) \qquad (2.15)$$

In each simulation step, the atoms interact with one another and the positions and velocities are updated. For short range interactions, a cut off radius is used to limit the number of interactions associated with each atom, therefore reducing the number of

computations. Atoms that are within the cut off radius are kept in the neighbor list, and only atoms in this list are used in the computations. This reduction decreases the time for simulation; however, if the neighbor list is updated too often, there will be computational cost associated with this operation which is undesirable. For this reason a buffer radius bigger than the cutoff radius is kept and the neighbor list is refreshed less frequently. The use of this buffer radius requires more memory use but reduces the time of computation to update the neighbor list.

LAMMPS uses its own scripting style in the form of an input file. First LAMMPS reads the input file, which contains information of the dimensions, units, boundaries, initial coordinates, time step, force filed parameters and execution instructions. LAMMPS then creates the atomic system and outputs the thermodynamics information on a log file. Additionally the atom coordinates are given for a certain number of time steps and can be visualized with additional software.

2.7 Simulations of carbon-ZnO interface

With the aim to better understand the mechanical properties between ZnO and carbon, a MD model has been developed to calculate the adhesive energy. In order to prepare the atomistic simulations, a model of ZnO independent of graphene was simulated. The initial model consisted of bulk material with periodic boundaries. After relaxation of the system, in other words, minimum energy and zero stress, the computation of basic properties was performed to validate the accuracy of the potentials like density and lattice energy. The second simulation was done with free surfaces normal to the Z-axis, since these surfaces are not naturally stable, they were stabilized before the calculation of adhesive energy. In order to stabilize them, ¼ of the Zn atoms

were removed according Tasker [35] and triangular voids were created. A stable configuration was obtained, and the VMD software was used to visualize the results of the simulation. This can be observed in Figure 2.3. The parameters provided in Table 2.1 and 2.2 were used in the simulation.

Table 2.1. Bonded interactions for the model of ZnO – graphene with functional groups, C=O, COH, COOH

Bond	Length (Å)	K/2 (kcal/ mol)	Bend	Angle (deg)	K/2 (kcal/m ol)
C-C (G)	1.40	234.5	C-C-C	120	31.5
C-H (G)	1.08	183.5	C-C-H	120	17.5
C-C^a (G)	1.51	158.5	C-C-C^a	120	35.0
C^a-C (K)	1.522	158.4			
C=O (K)	1.229	285.0			
C-O (H)	1.410	160.0	C-O-H	108.5	27.5
O-H (H)	0.945	276.5			
C=O (C)	1.229	285.0	O=C-O	121	40.0
C-O (C)	1.364	225.0	C-O-H	113	17.5
O-H (C)	0.945	276.5			
Torsion	K	D	N		
	3.625	180	2		
Improper	K	Xo			
	1.10	0.0			

C^a is the anchor carbon on the basal plane

() denotes G-graphene, K-ketone, H-hydroxyl, C-carboxylic acid

Table 2.2 Non bonded interactions for the model ZnO – graphene with functional groups C=O, COH, COOH

	Atom	σ(Å)	ε (kcal/mol)	q(e)
Graphene	C	3.4	0.0556	0.0
	C[a]	3.4	0.0556	0.08
Interface	C-Zn	2.92	0.4474	
	C-O	3.29	0.0924	
COOH	C	3.75	0.1049	0.55
	=O	2.96	0.2099	-0.50
	O	3.0	0.1700	-0.58
	H	0.0	0.0000	0.45
COH	C	3.4	0.0556	0.08
	O	3.07	0.1700	-0.70
	H	0.00	0.0000	0.435
C=O	C[a]	3.4	0.0556	0.08
	C	3.75	0.1050	0.47
	=O	2.96	0.2100	-0.47
Buckingham parameters				
	Pair	A	C	R
	Zn-Zn	220190.498	738.007	0.21916
	O-O	0.0	0.0	1e-10
	Zn-O	12216.328	0.0	0.3581

The MD model of the interface consists of ZnO slab with free surfaces, and a single layer of graphite (graphene) at the bottom of the ZnO slab. ZnO was constructed with periodic boundary conditions in the X and Y directions to give stability to the relaxed structure. The Z direction is not periodic and was stabilized considering two cases of the polar surfaces. First, ¼ of Zn atoms were removed from the Zn terminated surface; while in the second case, triangular voids were formed at the (0001) surface [49]. The edges of

the holes have oxygen atoms and the dimension of the edge was 9.3 Å. In both cases, a stable configuration was achieved. The dimensions of the structure was 42 Å x 38 Å x 20Å. In the first case with one fourth of the Zn atoms removed, the ZnO model has a total of 2912 atoms and in the second case with triangular voids a total of 2765 atoms. ZnO has multiple nonpolar surfaces, in these surfaces there is no divergence of energy at the surface, thus is possible to simulate the structure without distortion if the ideal wurtzite crystal. Simulations were also performed on the (1100) nonpolar surface, with the model having 2912 atoms.

In order to achieve a stable configuration of graphene, the edges were terminated by hydrogen atoms. This condition also allows graphene to achieve zero residual stress in the lateral directions independent of the size of LAMMPS simulation box. The dimension of the graphene layer was 32 Å by 28 Å, which is slightly smaller than that of the ZnO slab. Since the simulation box is adjusted to the size of ZnO, both ZnO and graphene have zero residual stress in the lateral direction independent of the mismatch in the dimensions of each structure. The residual stress may also be eliminated without hydrogen atoms on the edge of graphene by increasing the size of the structures until the dimensional mismatch becomes insignificant. However, this technique increases the computational cost without improving the accuracy of the simulation and was not evaluated here.

In order to validate the accuracy of the potentials, the first step is to calculate the properties of each structure in the stable, isolated form. Bulk ZnO was simulated resulting in a lattice energy of -39.34 eV and density of 5.65 g/cm^3. Graphene was simulated, and upon relaxation, the lattice cohesive energy was 8.65 eV/atom and in

agreement with known values [54,55]. The ZnO and graphene structures were then combined into a single model with a total of 3270 atoms and relaxed together in order to achieve zero global stress. The NPT ensemble [47] was used to obtain zero stress at the X and Y boundaries of ZnO. Specifically, the temperature was set to 100 K, and the system was simulated for 20 ps with the temperature gradually reduced to 1 K in the interval of 20 ps while keeping the NPT ensemble. The canonical ensemble (NVT) [45,46] was used to keep the volume constant and temperature of about 1 K for 20 ps.

After relaxation, the NVT ensemble was used to keep the temperature constant, and a displacement was applied to the graphene to simulate liftoff. The positions of the atoms at the top of ZnO were fixed in space; these atoms are shown in the shaded area of Figure 2.3. The graphene was then separated in the negative Z-direction while the rest of the ZnO atoms were allowed to deform through the interaction forces with the graphene layer. During the simulation, the stress on the graphene was recorded while the layer of graphene was displaced in steps of 0.25 Å. The structure was allowed to equilibrate for 20 ps between each step to yield a test velocity of 1.25 m/s. The stress on graphene during the liftoff is shown in Figure 2.3. The first step of separation generated an adhesive force of 9.8 nN, which rose rapidly in the subsequent steps to achieve a maximum adhesive force of 14.7 nN at 0.75 Å of separation. The force then begins a more gradual decline and is approximately zero nN at 7 Å. For the polar surfaces, both ZnO stabilization cases were considered, the case with one fourth of the Zn atoms removed and the triangular void stabilization, and the results obtained were the same. For the (1100) nonpolar surface, the separation simulation was performed with nearly the same results as the polar surface, thus showing that the inert surface of graphene does not

have a preferential interaction with the surfaces of ZnO. However this may not be the case if carbon has functional groups, since these could have different interaction on the deformed ZnO polar surfaces. The interface energy was calculated by integrating the force displacement curve to yield a total liftoff energy of 2.734 aJ. Normalizing by the area of the graphene surface (896 $Å^2$) gives a specific liftoff energy of 0.303 J/m^2.

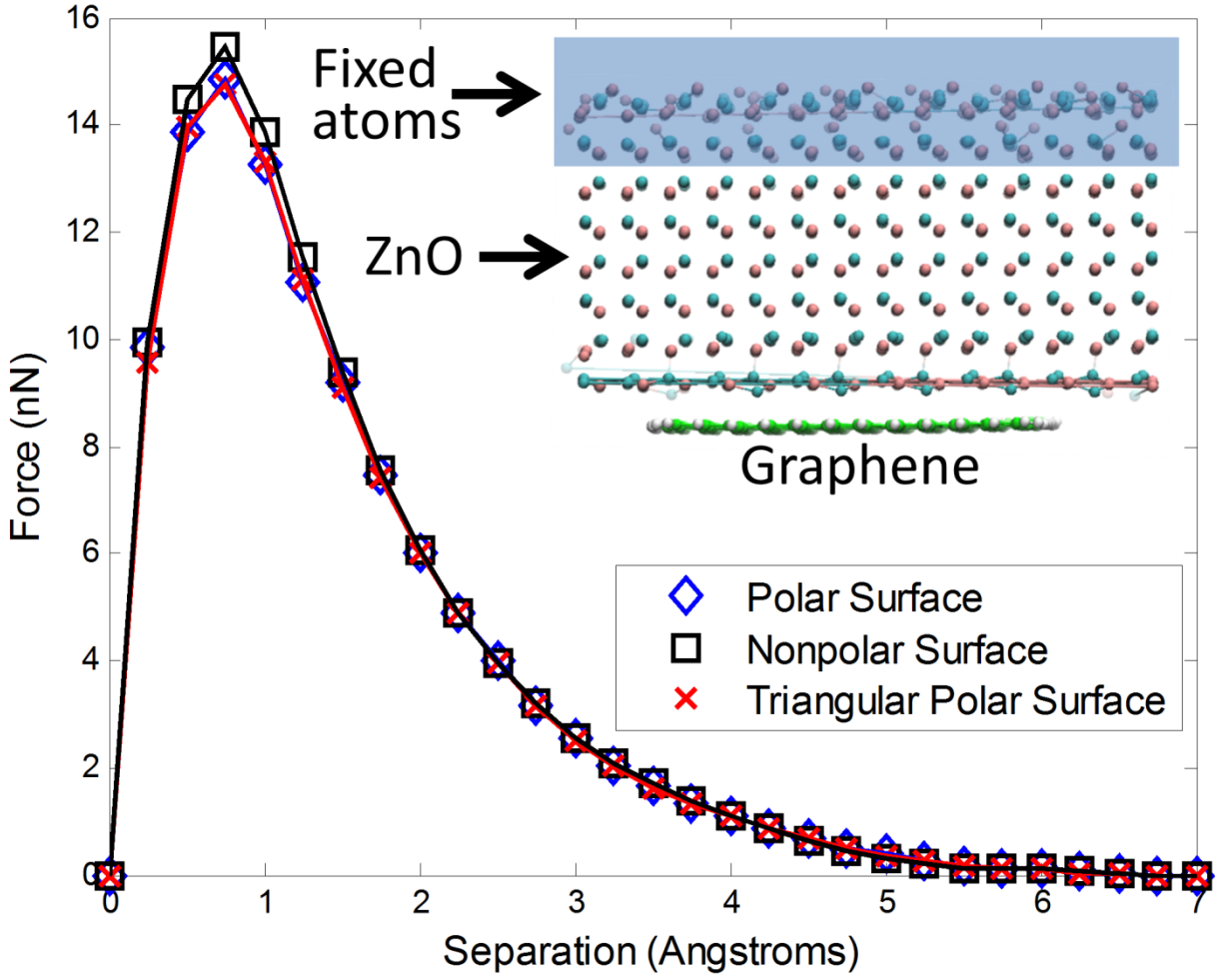

Figure 2.3. Force displacement curve on carbon atoms for the separation between the two materials as calculated with LAMMPS.

Molecular dynamic simulations have been used to study the behavior of material interfaces. The results clearly show that the interface between ZnO and carbon has good

adhesive properties and show how the materials deform upon loading as observed in the force displacement curves. From this study, it can be concluded that this simulation technique can be used to study other materials as long as the force fields of the interface are known.

2.8 Simulation of oxygen functional groups on carbon surface

Three types of functional groups, each corresponding to the primitive functional group, were simulated on graphene with surface concentrations of 1.6%, 3.3%, and 5%. The same procedure was followed to calculate the adhesive energy for each functional group and coverage fraction. Figure 2.4 shows the interfacial energy computed for each of the MD simulations. The interfacial energy is insensitive to the relative coverage of the hydroxyl functional groups and carboxylic acid functional groups. Both hydroxyl and carboxylic acid functional groups include hydrogen atoms, which can interfere with the ability of the ZnO to interact with the surface. Ketone groups contrast with hydroxyl and carboxyl groups in that they do not have any hydrogen atoms to interfere with bonding and have access to strongly interact with the Zn atoms in the ZnO crystal. Figure 2.4 shows that the interfacial energy increases with the fraction of functional groups and that the addition of ketone functional groups can increase interfacial energy beyond what is achievable with pristine graphite or the other classes of functional groups. This trend is consistent with the experimental observations that showed increases in the interfacial shear strength correlate with increasing ketone functional groups measured by XPS [36]. These simulations show qualitatively that there is a preference of ZnO to interact with ketones groups and, by controlling the amount of these functional groups, the adhesive energy between carbon a ZnO can be changed.

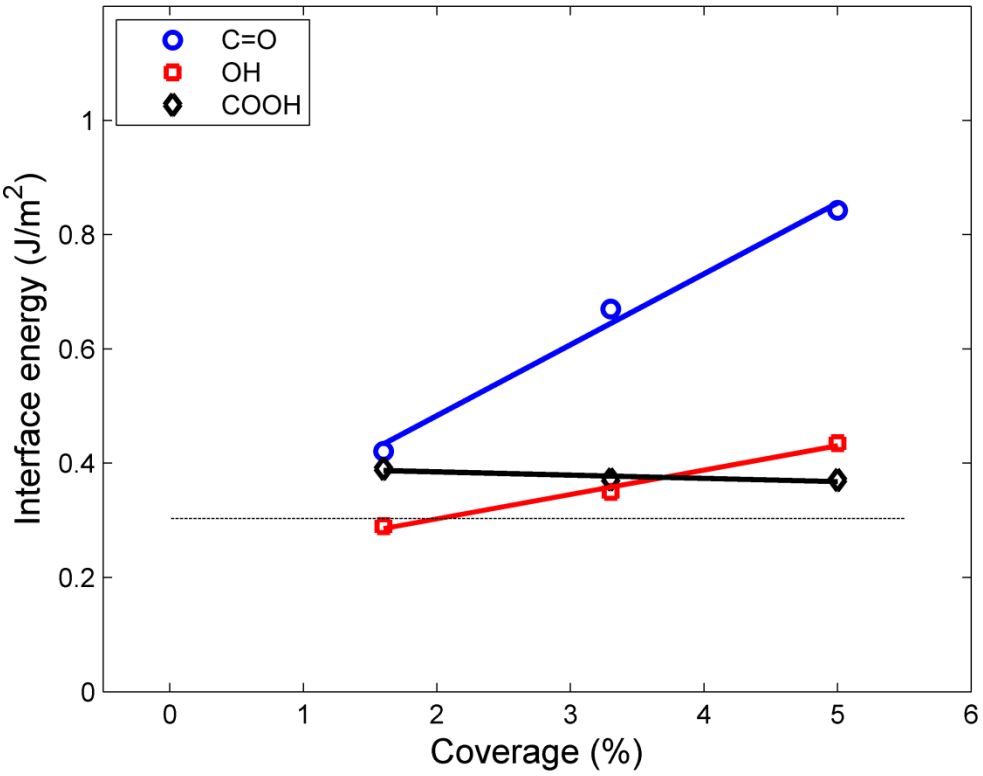

Figure 2.4. Molecular dynamics simulations of the adhesive energy between oxygen functional groups on graphene and ZnO.

CHAPTER 3

MEASUREMENT OF ADHESIVE ENERGY THROUGH ATOMIC FORCE MICROSCOPY LIFTOFF TEST

Following the theoretical study of the interface between ZnO and carbon, experiments were performed on the atomic force microscope (AFM) to directly measure the adhesive properties of these two materials. The extreme sensitivity of an AFM makes it possible to measure forces based on the atomic interaction between two materials [56] which defines the adhesive properties of the interface [57]. An AFM measures the displacement of the cantilever with great accuracy which combined with the cantilever's spring constant can be used to measure the force between the cantilever's tip and a surface. This force represents the balance between the cantilever's bending force and the atomic forces at the AFM tip substrate interface. By varying the properties of the tip and the surface, experiments can be performed to provide more insight into the molecular interactions and adhesion at a materials' surfaces. Thus, AFM has been applied to the characterization of polymer chains like poly-N-succinimidyl acrylate (PNSA) as well as the identification of properties that give rise to molecular interactions. For example, AFM gives high resolution when measuring the unfolding behavior of individual protein molecules [58]. In this application, the force on a single protein can be applied very accurately to control the rate of unfolding. This rate increases exponentially with the applied force, and thus, it is possible to obtain information about folding free energy, transition state and folding landscape. Furthermore, AFM allows the characterization of surface forces that dictate adhesion such as electrostatic and chemical forces [57]. With the ability to characterize bonding at an interface, AFM liftoff is useful for the study of how functionalization

treatments impact adhesive energy [59], allowing researchers to measure bond rupture forces [60] and adhesive mechanical forces [61]. In this chapter the AFM will be used to perform liftoff testing to measure the adhesive energy and to identify the characteristics of ZnO and carbon that lead to high interface strength.

3.1 Force displacement measurement

When using an AFM, the accuracy of the force measurement is limited by the uncertainty in the spring constant of the AFM cantilever, since this is used to relate displacements to atomic forces between the tip and the substrate. In order to reduce the uncertainty of the measurements in the experiments performed here, a cantilever probe calibrated according to the method by Sader [62] (MikroMasch, San Jose, CA, USA spring constant of 0.117 N/m ± 5%) was used in a Park XE-70 microscope. The second source of uncertainty in the measurement arises from the surface area of the tip, which must be known to determine the interface energy. Since the as-received tip has a radius of approximately 10 nm and the cantilever is mounted at a downward angle, it is necessary to flatten it in such a way that the surface is parallel to the substrate. In order to create a known surface area, the tip was scanned across a diamond lapping film (Model 50-30075 with average roughness of 11.14 nm) for several hours, which creates a flat surface parallel to the substrate and thus accounts for the slope of the cantilever.

3.2 Preparation of the AFM tip

3.2.1 Surface roughness

Given the difficulty of the task, roughness measurement was not made directly on the surface of the AFM tip; however it was made on the diamond lapping film giving an average roughness of 11.14 nm with standard deviation 17.87 nm. The topography and

histogram of the lapping film can be observed in Figure 3.2a and 3.2b respectively. It can be expected that the tip will have similar roughness, as the section 3.3 will show there is a minimal variation in the measurement of the adhesive energy caused by the tip roughness. After this step, the surface area of the tip was calculated using image analysis software on a Field Emission Scanning Electron Microscope (FESEM) image and the area was measured to be 0.067 μm^2 with ImageJ software as shown in Figure 3.1. Although a calibrated AFM cantilever was used for these experiments the stiffness value still contains approximately ±5% error [62], therefore the same tip was used through all experiments to ensure that the relative change in adhesive energy is accurate even though the absolute value will contain error.

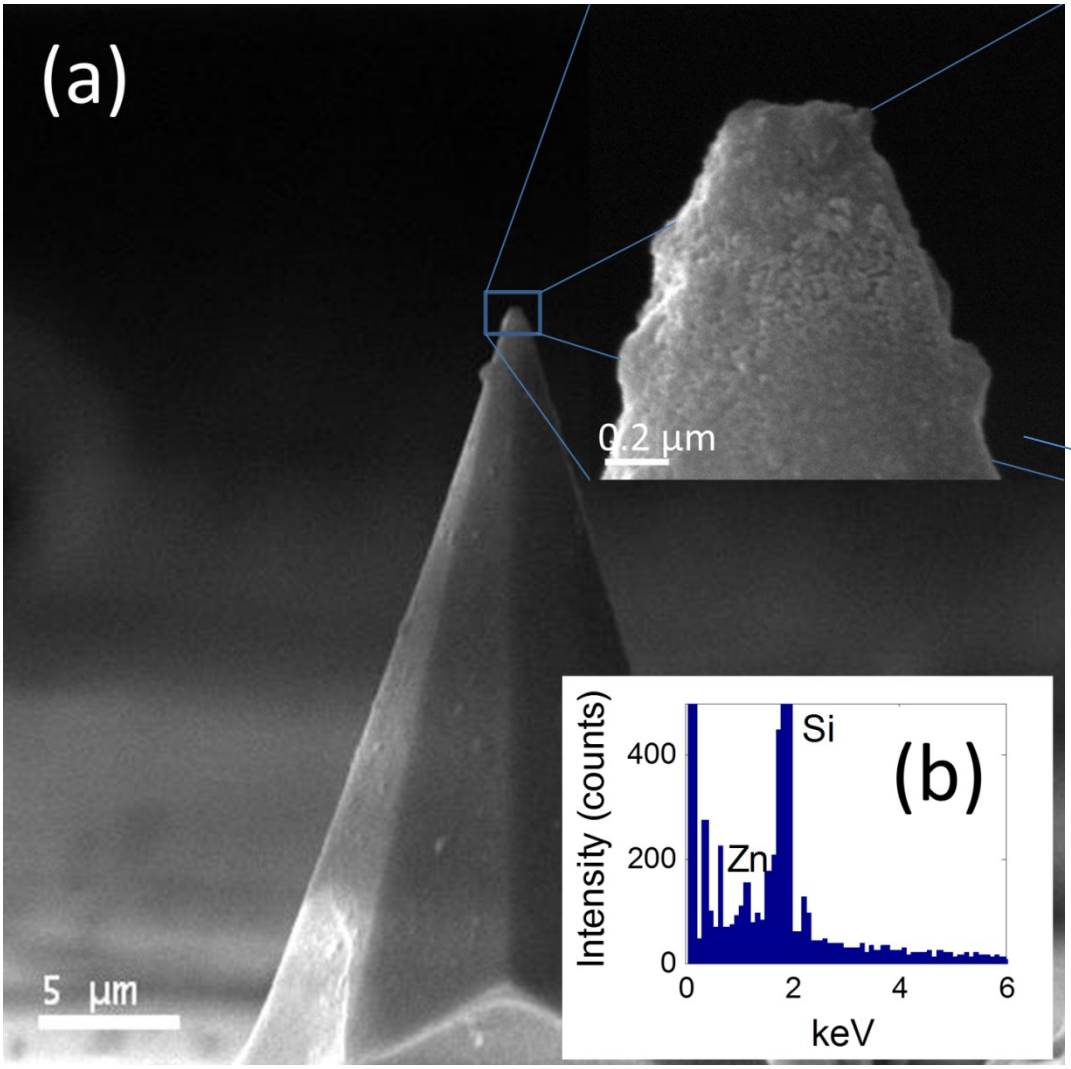

Figure 3.1 AFM tip for liftoff test a) flat surface of AFM tip with ZnO nanoparticles film b) EDX showing Zn.

3.2.2 ZnO nanoparticles

A thin conformal ZnO film was deposited on the tip surface through the deposition and coalescence of ZnO nanoparticles. The ZnO nanoparticles were synthesized following the method of Hu et al [63] to obtain a stable colloidal suspension of nanoparticles. The synthesis of ZnO quantum dot seeds is accomplished as follows: 1 mmol of zinc acetate dihydrate (Sigma Aldrich, 99%) was dissolved in 80 mL of ethanol

at 50 °C and vigorously stirred for 5 min. A separate solution of 2 mM sodium hydroxide (VWR, 97%) was dissolved in 100 mL of ethanol at 50 °C and stirred vigorously for 5 min. Both solutions were then cooled to room temperature. Upon cooling, 40 mL of zinc acetate solution was added to 320 mL of ethanol, and 40 mL of sodium hydroxide solution was added to 100 mL of ethanol. The solutions were heated separately to 65 °C then mixed together under vigorous stirring while maintaining the temperature at 65 °C for 30 min.

Once the colloidal solution was prepared, the AFM tip was dipped into the solution and then put into an oven at 70 °C for 3 minutes. This process was repeated seven times to form a thin layer of ZnO on the tip to mimic the surface of the ZnO nanowires. The presence of a continuous ZnO film on the surface of the AFM tip was confirmed through the use of SEM analysis and energy dispersive X-ray (EDX) analysis. An image of the flattened and coated tip as well as the EDX data is provided in Figure 3.1. In the case of ZnO, the measurement of the roughness was made indirectly, ZnO nanoparticles were deposited on mica following the same method that the AFM tip. The topography and histogram are shown on Figure 3.2c and 3.2d respectively; here the average roughness was 0.664 nm with standard deviation 1.06 nm.

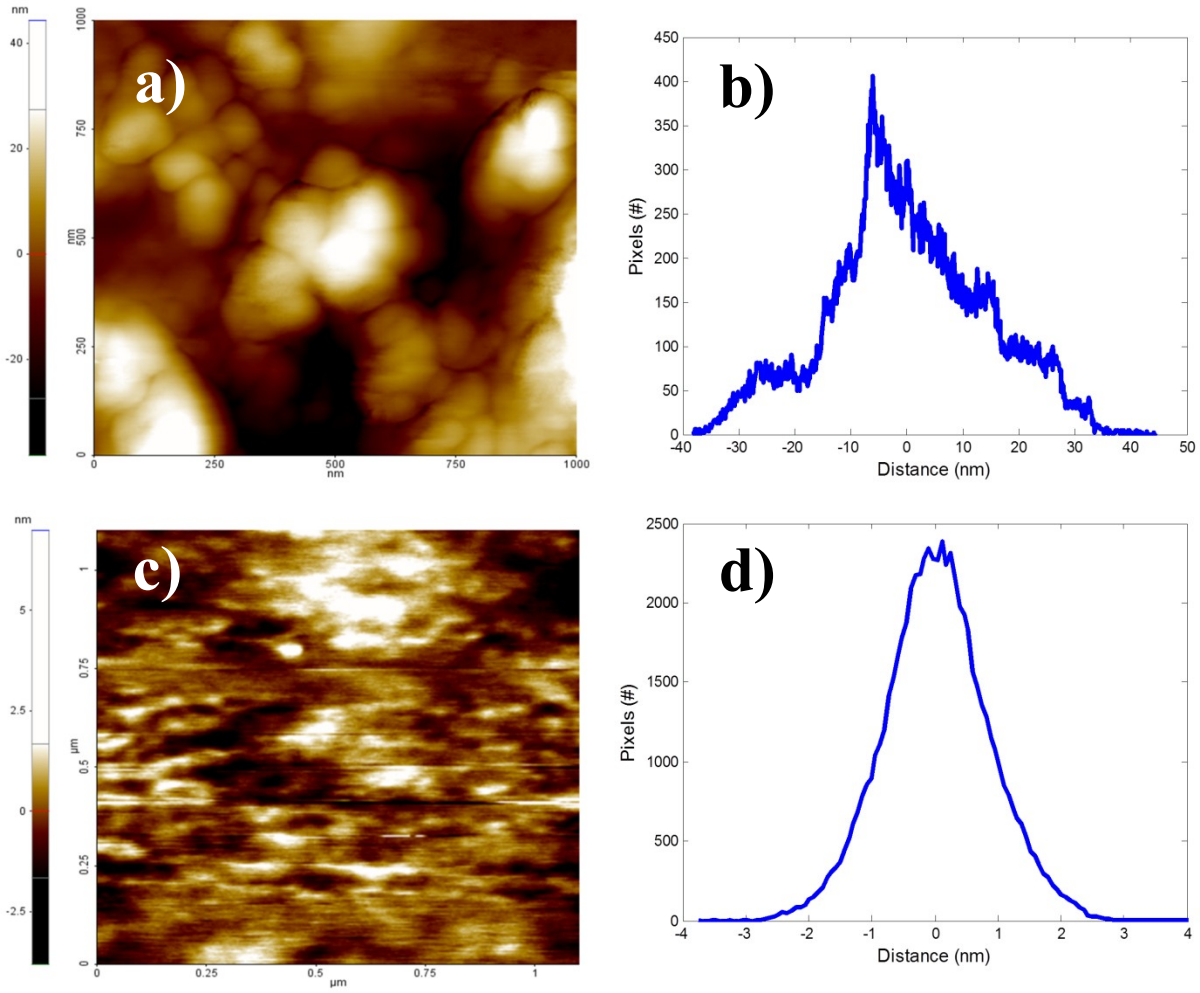

Figure 3.2 Roughness measurements (a) Topography of diamond lapping film, (b) histogram corresponding to the topography of the diamond lapping film, (c) Topography of ZnO film deposited on mica, (d) histogram corresponding to topography ZnO film.

3.3 Test of adhesive energy between ZnO and carbon through AFM liftoff

Once the tip was coated with ZnO, force displacement measurements were taken under the AFM with a fresh HOPG surface. In this test the AFM tip approaches the surface of HOPG with a small force that deflects the cantilever allowing intermolecular interactions between the substrate and the tip surface. The cantilever is then retracted to separate the tip from the substrate, however due to intermolecular forces between the

AFM tip and the substrate, the tip does not separate immediately but instead it deforms due to adhesion. In other words the AFM cantilever beam stores all of the potential energy needed to separate the surfaces before the interface fails with an abrupt change in force. This deformation of the cantilever is precisely measured and recorded by the AFM data acquisition system which can be correlated to the adhesive force. At the end of the test, the tip separates from the substrate and the force drops to zero. The displacement can be related to intermolecular forces by utilizing the known stiffness of the cantilever beam and the adhesive energy is calculated from the force displacement curve [56,57] which is the shaded area in Figure 3.3b. The specific adhesive energy is obtained by dividing by the contact area. The adhesive energy between HOPG and the bare tip was 0.087 ± 0.0071 J/m^2 as shown in Figure 3.3a (blue squares), the small variation in this set of measurements indicates that the roughness of the tip has a small effect in the calculation of the adhesive energy.

The presence of ZnO on the AFM tip produced a higher energy of adhesion as shown in Figure 3.3a. The force measured at the moment of separation in the AFM was 66.53 ± 7.46 nN. As a calibration of the testing procedure, the ZnO layer was then removed using an 1.23 M HCl solution, and the testing was repeated, producing the same adhesive energy prior to coating with ZnO. This both demonstrated the repeatability of the test as well as the validity of the approach. A layer of gold was sputter coated on the top of the cantilever to serve as a reflective surface that is unaffected by the acid cleaning. The tip was then recoated with ZnO using the same process and the interface energy was measured followed by removal of the ZnO from the tip in acid and testing on a clean HOPG surface. The measurements were confirmed by repeating this process three

additional times, with the mean for each set of tests shown in Figure 3.3a. The average value for the energy of adhesion as calculated from the force displacement curve was 0.261 J/m^2 with a standard deviation of 0.054 J/m^2 for the ZnO HOPG interface. The variation of the measurement could be caused by the uniformity of the ZnO nanoparticles deposited in the AFM tip; however the liftoff testing demonstrates the strong adhesive energy between ZnO and HOPG

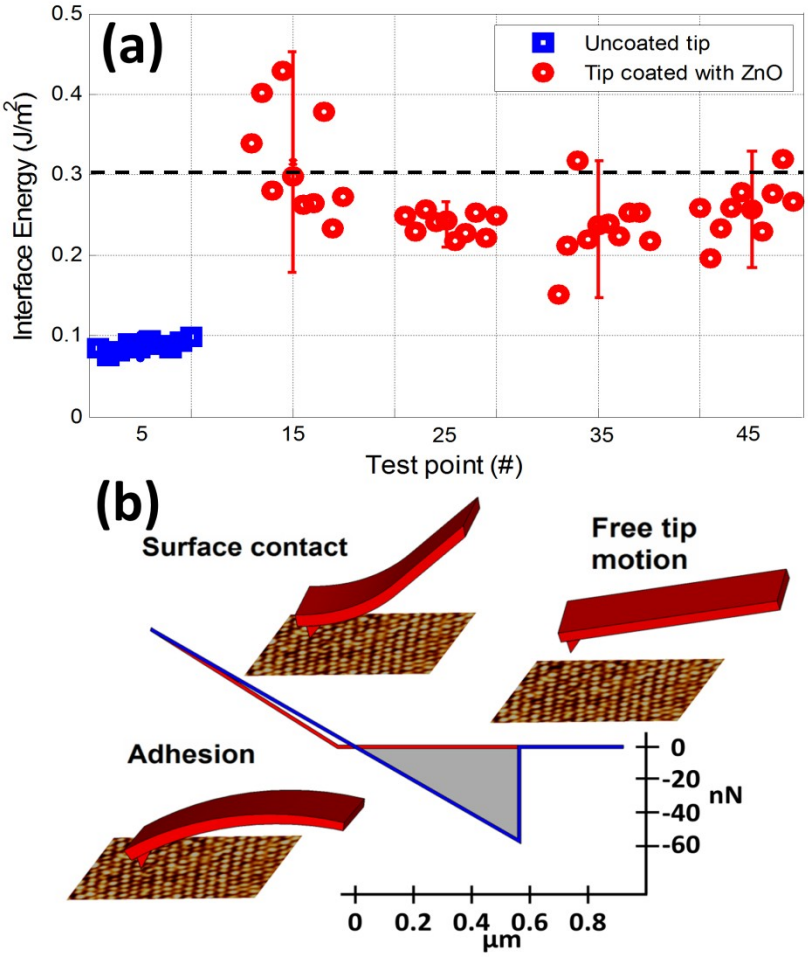

Figure 3.3 AFM liftoff test a) results for the coated and uncoated AFM tip, b) typical force displacement curve.

To understand the difference in adhesive energy between Si-HOPG and ZnO-HOPG, it is important to look at the properties of ZnO and Si. The primary difference is that ZnO has ionic bonding caused by electrostatic forces, while Si is covalently bonded. In the ZnO crystal, the addition of electrostatic energy in the *c* axis causes the energy to diverge at the polar surface [35], thus a stabilization mechanism takes place.

On the other hand, Si is a covalently bonded material, with symmetric configuration on the surfaces [64]. The results of the AFM test suggest that the higher adhesive energy between ZnO and HOPG is caused by forces other than just van der Waals interactions. In general, these are known as non-bonded interactions such as long and short range interactions. This type of force is known to increase adhesion and in some cases the attractive forces can be as large as cohesive forces in covalent-ionic solids. [65] In the case of Si the adhesion energy will come only from Van der Waals forces since Si and HOPG are two covalently bonded materials. And finally the measurements performed with the AFM are in agreement with known values of Van der Waals adhesive energy, which is typically < 0.11 J/m^2.

3.4 Effect of oxygen content on adhesive energy

Also in the study of the properties of the interface of carbon fibers, it has been demonstrated that the strength can be changed by controlling the chemical composition of the fiber's surface. The interfacial shear strength increased with an increase in the oxygen content on the surface of the carbon fiber [36]. As the results of single fiber fragmentation (SFF) testing suggested, the oxygen functional groups present at the surface of the carbon fiber have favorable intermolecular interactions with ZnO nanowires which leads to higher adhesion energy and consequently higher interfacial

shear strength. However, all these the experiments do not directly evaluate the adhesive properties of the ZnO – carbon fiber interface strength because in the SFF test the fiber is embedded in a polymer matrix and the interfacial shear strength is calculated based on the number of fiber fragments formed during the test. In order to study the behavior of this interface in more detail, this dissertation uses atomic force microscopy to quantify the adhesive energy between ZnO and an oxidized graphite surface by previous AFM liftoff testing method to measure the adhesive energy of the HOPG - ZnO interface.

3.4.1 HOPG functionalization

HOPG was used to represent the carbon fiber surface and it was functionalized through exposure to an oxygen plasma such that a range of oxygen groups (i.e. C-OH, C=O, C-O-C, COOH, etc.) were generated as on the surface of a carbon fiber [66]. The functionalization of HOPG samples were adjusted by plasma treated in a PSI Plasma Prep II at 100μinHg pressure for 15, 30 and 60 seconds in an oxygen atmosphere (99.6% purity) and 20W of power. It is known that the oxygen functional groups on carbon surface will be increased after plasma treatment [67]. In order to determine the chemical composition of the functionalized HOPG samples, they were analyzed by X-ray photoelectron spectroscopy (XPS) using a Perkin Elmer 5100 XPS system. The XPS data was analyzed with the aid of CASAXPS using the built in Marquette regression function. Each dataset was fit with a Gaussian 70% - Lorentzian 30% curve mixture (GL30), that were constrained in location and full width at half maximum (FWHM). All peaks had a constrained FWHM of 1.1-1.7 eV and were constrained at location of 284.5-285.5 eV, 285.5-287.0 eV, 286.5-288.0 eV, 288.0-290.0 eV and 291-293 eV for C-C, C-OH, C=O, C-OOH and π-π C-C bonds, respectively. Figure 3.4 clearly shows the high

resolution C1s spectrum which demonstrates increasing oxygen content and the change of chemical composition by covalent bonding between carbon and oxygen atoms which results in the formation of different chemical species.

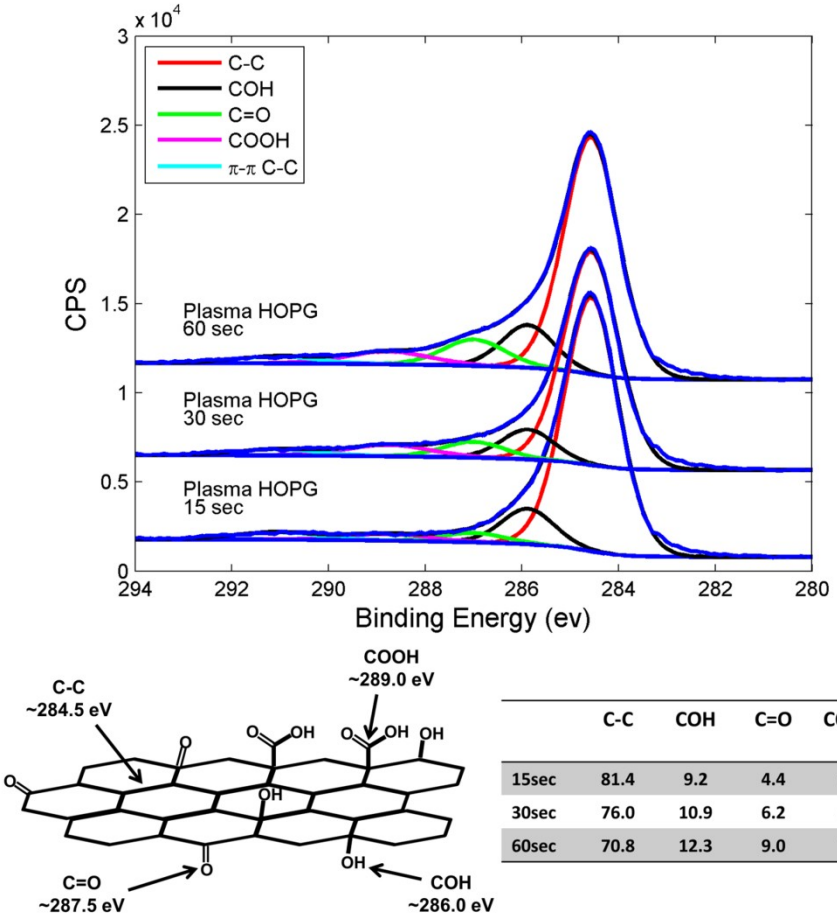

	C-C	COH	C=O	COOH	π-π
15sec	81.4	9.2	4.4	4.0	0.9
30sec	76.0	10.9	6.2	6.0	0.8
60sec	70.8	12.3	9.0	7.1	0.7

Figure 3.4 X-ray Photoelectric spectroscopy of plasma treated HOPG showing the creation of functional groups.

3.4.2 Adhesive energy of plasma treated HOPG.

After the functionalization procedure, the HOPG samples were tested through AFM liftoff and the results are shown in Figure 3.5. Each data point represents a single measurement, and at the end of each set of measurements i.e. after 15 data points, the tip was cleaned in acid and recoated with ZnO prior to a change in the substrate following

the procedure described in section 3.3. As can be clearly observed in Figure 3.5, the adhesive energy increases as the oxygen content increases. The magnitude of the interaction between the functional groups and the surface of ZnO suggest that interaction forces are not only van der Waals but also could be electrostatic and induced forces [68]. More important, this suggests that ZnO binds to ketones, carboxylic acid and hydroxyls and these groups can change the adhesive force between carbon and ZnO.

In the case of hydroxyl groups, they can form hydrogen bonding and given that ZnO hosts OH groups, interactions can arise at the interface [69]. In carboxylic acid, there is a bond angle of 120 degrees between the carbon and oxygen atoms. Because this bond angle is fixed, it is necessary to match the interaction of the hydrogen and oxygen atoms which form a planar structure. This planar structure has been shown to interact with other planar structures, allowing the formation of a network [70]. Since none of the ZnO surfaces have planar structure it is possible that this carboxylic acid does not contribute towards increasing the adhesive energy, thus it could be inactive at the surfaces of ZnO. Ehlert et al. observed a similar finding with carbon fiber where the relationship between the surface content of carboxylic acid groups and the interfacial strength showed little correlation. Furthermore, it has been reported that the orientation of ketones can change depending on the binding with other molecules [71], with the flexibility of ketones to change orientation, this could facilitate the interaction with ZnO leading to high interaction forces.

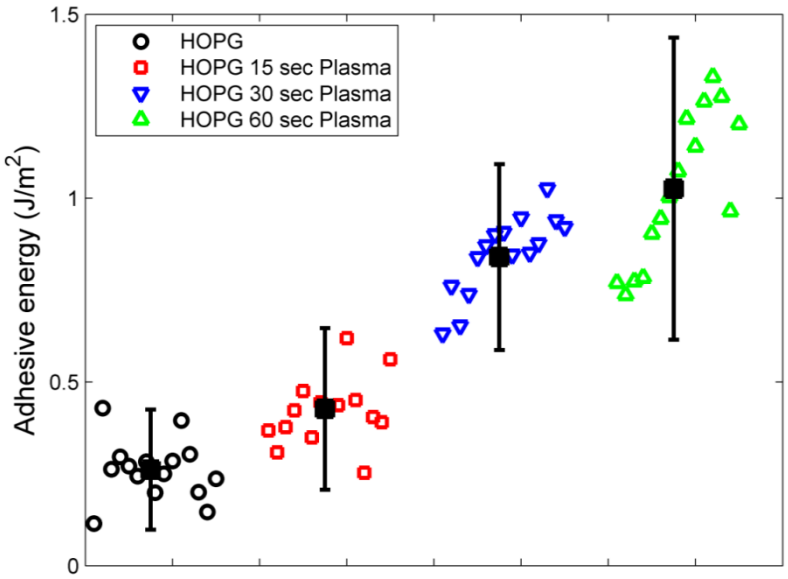

Figure 3.5 AFM test showing the adhesive energy between functionalized HOPG and tip covered with ZnO

On the other hand ZnO is an ionic material, and it has important adsorption properties, for example, different molecules can interact and be absorbed at the surface. The polar surfaces on ZnO tend to deform and interact with other molecules making them chemical active and this can be a cause for the strong intermolecular interactions with the functional groups present on the HOPG surface [49]. The wurtzite structure is also dominated by the nonpolar $(10\bar{1}0)$ plane which consists of Zn–O dimer rows, and the oxygen and zinc ions are tetrahedrally coordinated. The $(10\bar{1}0)$ plane show a tilt and the oxygen atoms are raised out on the surface, thus giving the possibility of hydrogen bonding interactions with surrounding molecules that are present at the surface of HOPG [72].

Even though there are non-bonded interactions at the interface, these results suggest that the intermolecular interaction caused by long range forces between ZnO and the

functional groups can be significant towards increasing the adhesive energy. These long range forces can arise because of the static charge distribution of the molecules resulting Coulombic interactions but also by the distortion of a molecule in the presence of neighbor molecules. As other researchers have observed [73], the magnitude of long range forces can be significantly larger than Van der Waals forces which typically lead to adhesive energy < 0.11 J/m^2 [65].

3.5 Intermolecular Interactions

The previous section has demonstrated that the non-bonded interaction plays an important role on improving high adhesive strength of the carbon. In order to elucidate more detail about the properties of carbon, the mechanism at molecular level is investigated here to bridge these interactions to the macroscopic properties of the material.

As the results will demonstrate, after ZnO is brought into contact with an oxidized graphitic surface, the ZnO film is charged suggesting the absorption of active oxygen species or electron transfer. The charged surface is retained after being removed from the functionalized surface and three different phenomena were observed: the charge is transferred to gold and indium conductive substrates, it does not transfer to HOPG and copper conductive substrates, and it polarizes the surface of HOPG and annealed silicon to create induced interactions that increase the adhesive energy. The results suggest that energy barriers between ZnO and the conductive substrate define if the charge is transferred, and the polarizability of the substrate along with the charge on ZnO film define the magnitude of the induced forces that affect the adhesive energy. By using this

approach the mechanism dictating the adhesion to graphitic surfaces can be identified and used to design interfaces.

In the course of the experimental testing, it was observed that the ZnO coated tip produced very high bonding with the pristine HOPG surface after being approached to a highly plasma treated HOPG surface. In other words, following contact with the highly functionalized HOPG surface, the tip's surface experiences a chemical reaction that allows it to further interact with other surfaces. Three separate cases were considered in which the tip was first brought into contact with plasma treated HOPG for either 15, 30 or 55 seconds at 100W of power and subsequently brought into contact and lifted off the pristine HOPG surface. Each liftoff test was done with a peak force of 40 nN and a speed of 0.3 μm/s followed by withdrawal of the tip at the same speed, and the points in Figure 3.6b represent an individual liftoff to show the repeatability. As the plasma time increases, and thus the surface content of oxygen groups increases, the adhesive energy between the ZnO and pristine HOPG increases from 0.26 J/m^2 for the as coated ZnO, to a mean value of 1.3 J/m^2 for the case when the tip was initially brought into contact with the most oxidized surface. This adhesive energy is much stronger compared to the bonding of typical polymers with graphite such as epoxy [74]. Furthermore, this test demonstrates that when the ZnO is brought into contact with the highly oxidized graphite surface there is a reaction that takes place leading to a modification of the ZnO surface.

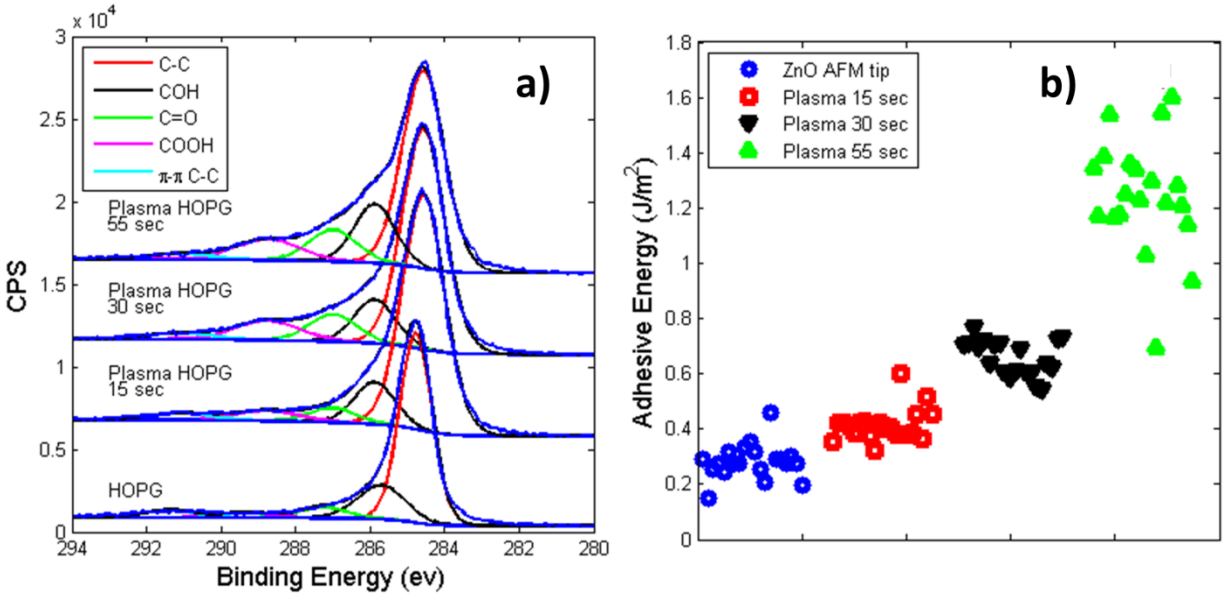

Figure 3.6 Intermolecular interaction between ZnO and HOPG a) XPS analysis of functionalized HOPG, b) AFM test of coated ZnO tip on HOPG.

The increased bond strength between the pristine HOPG and the ZnO coated AFM tip following contact with an oxidized graphitic surface was believed to be caused by an electron transfer from the electron rich functionalized graphite to the ZnO. This hypothesis was evaluated through liftoff experiments on both positively and negatively charged substrates and thus could validate the surface charge on ZnO. Silica glass was chosen as the substrate and was negatively charged by soaking it in piranha solution (30% hydrogen peroxide and 70% sulfuric acid) for 30 minutes at room temperature [75]. Then, the substrate was rinsed with Milli-Q water under ultrasonic agitation and finally it was cleaned with acetone and ethanol and rinsed with Milli-Q water. To obtain a positively charged surface [75], the negatively substrate was immersed in a 1% poly diallyldimethylammonium chloride (PDDA) v/v aqueous solution for 5 minutes and then

rinsed with Milli-Q water, thus creating a layer of PDDA with positive charge on the surface through electrostatic self-assembly.

Liftoff testing was performed against these negatively and positively charged surfaces with the ZnO coated tip after it contacted functionalized HOPG, and the results are plotted in Figure 3.8a. It can be observed that the tip had low adhesive energy when tested on the negatively charged surface and high adhesive energy with the positive charged surface, thus this indicates the presence of a negatively charged surface of ZnO on the AFM tip. This result agrees with the hypothesis that the ZnO coated tip obtained a negative charge when it was brought into contact with the surface of the functionalized HOPG, and that this surface charge on the ZnO coated tip increased the adhesive energy when subsequently contacted to the pristine HOPG. It is interesting to note that this charge is not dissipated when the AFM tip is brought into contact with the conductive pristine HOPG and the charge can be maintained on the tip after washing, thermal treatment under vacuum, and when held under vacuum for extended periods of time. This charge stability indicates that there may be further intermolecular interactions in play, more specifically, this suggests the existence of induced forces between the AFM tip and HOPG.

With the bonding interaction controlled by the charge on the AFM tip, it is important to know the conditions required to maintain the charge and to demonstrate the mechanism by which this charge is preserved when in contact with HOPG. In order to show this, the adhesion of the charged ZnO tip was evaluated with gold, indium and copper substrates through AFM liftoff. In these metal materials the electron energy levels of the conduction band and the valence band overlap and exited electrons can jump

into the conduction band where they are free to move inside the material. Thus, this gives the possibility of electron transfer from the charged ZnO tip to the substrate. However, it is know that ZnO can form ohmic or Schottky contact dependent on the work function and electron affinity of the material with respect to ZnO.

The ohmic contact is characterized by its linear relationship between current and voltage and no energy barrier; under the conditions of the experiment it can be expected charge transfer from ZnO. In order to demonstrate this effect the charged AFM tip is brought into contact with gold which is known to form an ohmic contact with ZnO [76,77]. Following contact between the charged ZnO AFM tip and gold, electrons were transferred to the substrate such that the ZnO lost its surface charge and upon subsequent liftoff with pristine HOPG, the tip exhibited weaker bonding as shown in Figure 3.7a. Similarly, it was observed the charge transfer after the charged ZnO tip touched the indium substrate, which is also expected since ZnO and Indium also form an ohmic contact [78,79].

Unlike the ohmic contact the Schottky contact exhibits an energy barrier which can prevent electron transfer below the barrier height, thus, it will be expected that the charge will remain on the ZnO AFM tip after approaching a substrate that forms a Schottky barrier. Since graphite and ZnO form a Schottky barrier charge transfer from the charged ZnO AFM tip to HOPG is not observed. Specifically Yastkiv et al [80] have reported the Schottky contact will have a 0.89 eV barrier height for the graphite/ZnO $(000\bar{1})$ contact and 0.60 eV for the Graphite/ZnO (0001) contact. Interestingly, it has been reported that ZnO and copper form an ohmic contact [81] or quasi ohmic contact with barrier height of 0.35 eV [82]. Furthermore, it is known the chemical composition at the interface can

affect energy barriers height, for example Schmidt et al [83] observed that the Schottky barrier height increased in the presence of an oxide layer between gallium arsenide and a copper interface. Since a copper oxide passivation layer forms on the surface of bulk copper, it is possible to create a Schottky barrier between ZnO and copper and use this interface to demonstrate that under Schottky contact the charge on the AFM tip is preserved. Therefore the charged ZnO coated AFM tip was brought into contact with a copper oxide surface and subsequently liftoff testing was used to evaluate the tips adhesion to HOPG. The resulting adhesion energy is provided in Figure 3.7b and clearly shows that unlike the ohmic contact with Indium or gold, the adhesive energy is preserved under the conditions of a Schottky barrier which is present between ZnO and HOPG.

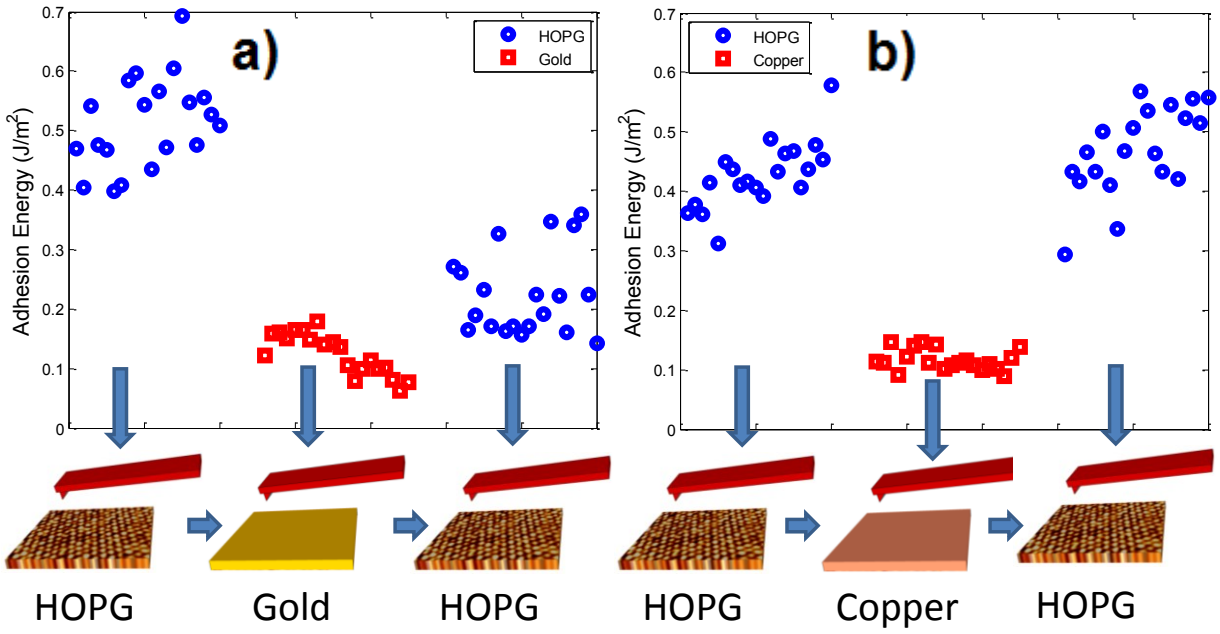

Figure 3.7 Test of charged ZnO coated AFM tip on conductive substrates a) the charge is lost on gold, b) the charge is not lost on copper.

It has been speculated that induced forces between HOPG and the charged ZnO AFM tip resulted in high adhesive energy. With the purpose to prove the existence of induced forces caused by the ZnO charged AFM tip, two different samples of silicon were prepared: the first one a cleaned single crystal silicon wafer and the second one silicon wafer annealed at 150 °C for 30 minutes. These two samples were tested with the charged ZnO AFM tip and the results are shown in Figure 3.8b. It can be observed that higher adhesive energy occurs with the silicon that was annealed at 150 °C. During the annealing process dangling bonds are created on the silicon surface [84], the presence of these dangling bonds lowers the energy gap between the bonding and antibonding orbitals, i.e. the HOMO - LUMO gap, and in consequence, the poilarizability increases [85]. The higher polarizability of the silicon substrate leads to higher induced forces in the presence of the AFM tip and results in a higher adhesive energy as shown in Figure 3.8b, this result confirms that the high adhesive energy observed on HOPG is caused by induced polarization forces given its relatively high polarizability [86].

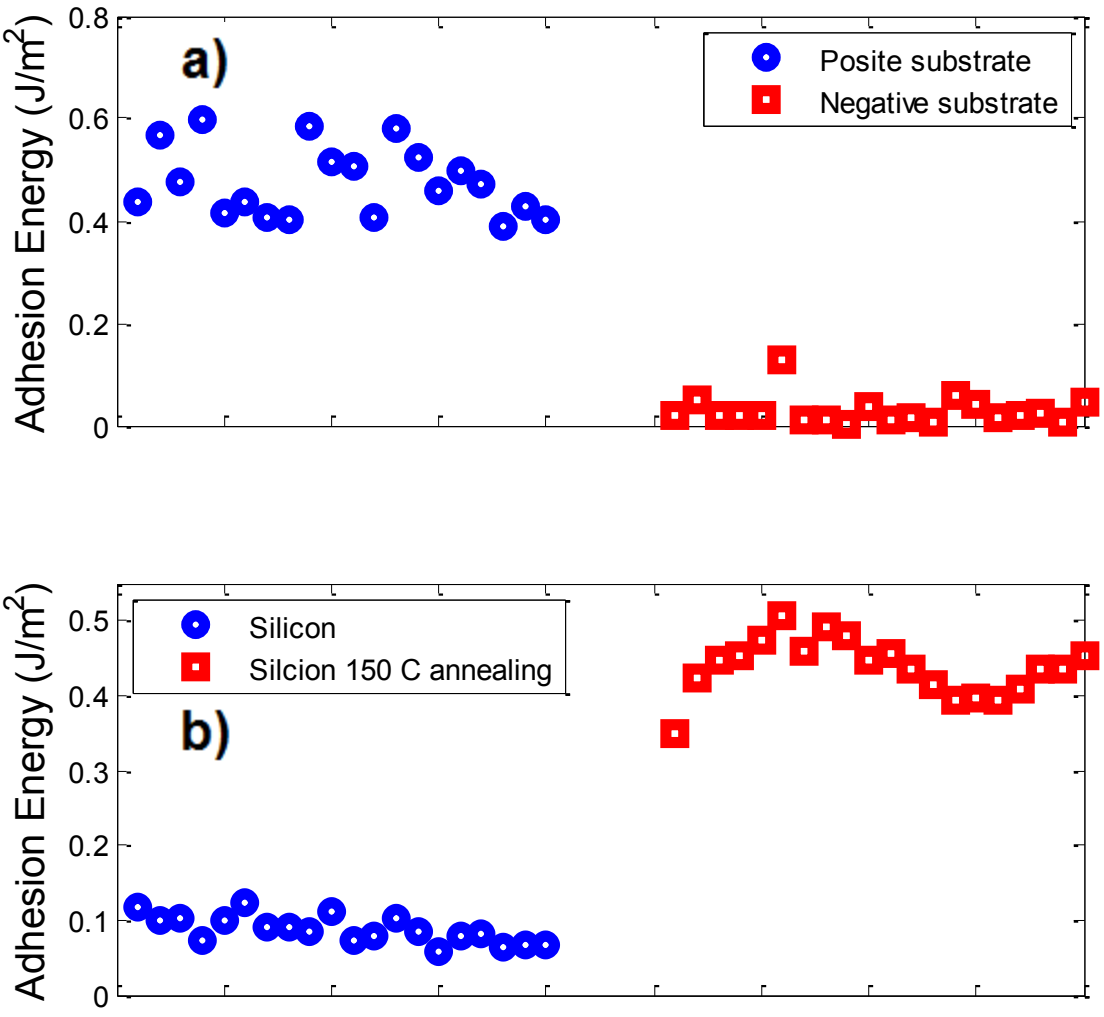

Figure 3.8 Liftoff test of charged ZnO coated AFM tip a) on negative and positive substrates, b) AFM tests on silicon and annealed silicon.

Through the AFM liftoff experiment, this dissertation has successfully quantified the intermolecular interactions present between ZnO and HOPG. Recent results have shown ZnO to strongly bond with carbon fiber surfaces in the absence of covalent bonding and thus the adhesive energy between ZnO and carbon fiber should be dictated by non-bonded interactions. Through the AFM liftoff technique it has been possible to quantify the intermolecular interactions present between ZnO and HOPG. The results presented

here can be used to understand the bonding across solid interfaces and may be applied to the design of high strength interfaces in a variety of applications, including carbon fiber surfaces, ceramics and polymers. It was found that ZnO obtains a negative charge after approaching the electron rich surface of oxidized sp^2 bonded carbon surfaces; it was also observed that the charged ZnO AFM tip maintains its charge if there is an energy barrier between ZnO and the conductive substrate but the charge is transferred in the absence of the energy barrier. The adhesive energy between pristine HOPG and a charged ZnO AFM tip was measures to be as high as 1.7 J/m^2. The high adhesion was demonstrated to result from the polarization of HOPG in the presence of a negatively charged ZnO surface and further demonstrated through the characterization of silicon surfaces of low and high polarizability.

CHAPTER 4

ADHESIVE ENERGY BETWEEN GRAPHITE AND WURTZITE MATERIALS

In chapter 3, it was shown that the adhesive energy between ZnO and carbon is a result of interactions stronger than Van der Waals forces. Since ZnO is formed by ionic bonding of the Zn^{+2} and O^{-2} ions [87] and carbon has relatively high polarizability, induction forces could be present at the HOPG-ZnO interphase that result in high adhesive energy. It was also shown that polarizability is important for adhesive energy, confirmed by the test of two silicon substrates with different levels of polarizability, showing a high increase in adhesive energy with an increase in polarizability. Consequently, ZnO will be substituted with materials with the same ionic characteristics but with higher polarizability. In this chapter materials other than ZnO to create an interphase will be presented, and it will be elucidated how the adhesive energy is related to polarizability of the ionic material. Like ZnO ionic crystals of the II-VI compounds exhibit wurtzite structure, however the crystals formed by atoms of bigger atomic mass have bigger unit cell volume and show trends in several other properties.

4.1 Introduction

It is hypothesized that other ionic materials such as cadmium selenide (CdSe), cadmium sulfide (CdS) and zinc sulfide (ZnS) could have higher adhesive properties than ZnO due to their higher polarizability. These materials also have a wurtzite crystal structure, but with different atomic mass and energy levels associated with the electron orbitals [88]. These differences lead to different materials properties, such as: lattice parameters, band gap, index of refraction, elastic constants and piezoelectric constants [89]. These materials do not have a symmetric center and consequently, these materials

exhibit piezoelelectric and polar characteristics [90]. Furthermore, it has been shown that the polarizabilty of a wurtzite crystal increases as the unit cell volume increases [91]. The relationship between unit cell volume and electronic polarizability can be explained by the fact that the electron cloud of an atom with large radii can be distorted easily as compared with one with small radii, thus leading to higher polarizability. The unit cell volume of these materials are: ZnO 43 $Å^3$ [92], ZnS 65 $Å^3$ [92], CdS 98.97 $Å^3$ [92], CdSe 112.24 $Å^3$ [92].

The polarizability of an ionic crystal depends on the polarizability of the individual ions, short range interaction that modify non local response, [93] and the interaction of the ions within the crystal [94]. Weak binding of the nuclei to the electrons and large delocalization tend to promote the polarizability magnitude, for this reason atomic systems with small polarizability are more stable than systems with large polarizability [95]. Since the polarizability is inversely proportional to the ionization energy i.e. the amount of energy required to remove an electron from an atom; then, the tighter the electron, the more difficult is to distort the electron distribution around the nuclei.

The polarizability of an atomic system is important for the formation of induced interactions. A polarizable atomic system can acquire a temporarily induced dipole moment as a result of the influence of an electric field generated by a nearby ion or polar system [96]. The field distorts the electron cloud and gives rise to an electric dipole. Since the magnitude of the induced dipole moment is proportional to the strength of the electric field and the polarizability $\mu^*=\alpha E$, the larger the polarizability, the larger the induced dipole moment, and the dipole moment also depends on the orientation of the molecular systems with respect to the electric filed. Thus, a polar system can induce a

dipole moment on a polarizable system (polar or nonpolar) because the charges of the polar molecule give rise to an electric field that distorts the polarizable system. In this case, the induced dipole formed on carbon interacts with the permanent dipole of the ionic material and the two are attracted together and this interaction is called induced-dipole dipole interaction [97].

In the previous chapter, the adhesive energy of ZnO-HOPG was tested, here the adhesive properties of ZnS, CdS, CdSe on HOPG will be tested following the same methodology with the Atomic Force Microscope (AFM), similar to the experiments on chapter 3. Nanoparticles will be synthetized and they will be used to create a film on the AFM tip, then the adhesive properties will be measured through AFM liftoff test.

Based on the results from the AFM liftoff test, CdS nanoparticles will be used on carbon fibers to tests the effect on the interface strength. As explained elsewhere [5,7,36], the synthesis of ZnO nanowires requires the deposition of a layer of nanoparticles. CdS nanoparticles will substitute ZnO nanoparticles to create a layer on the surface of carbon fiber, then ZnO nanowires will be grown on the nanoparticle surface and the interface strength will be evaluated through single fiber fragmentation test. Two different sets of samples will be analyzed, the first set with only ZnO film on the fiber and the second one with CdS film on the fiber in order to evaluate the effect of the CdS nanoparticles on the interfacial shear strength.

4.2 Synthesis of nanoparticles

Since CdS ZnS and CdSe nanoparticles can be thermodynamically unstable, agglomeration can be initiated in the synthesis and many efforts have been devoted to develop methods to control growth of these types of nanoparticles to provide suitable

conditions for the growth [98]. Among the various methods to produce nanoparticles, microemulsions [99] have been widely used to synthetize several type of nanoparticles, the microemulsions are thermodynamically stable isotropic mixtures of water, surfactant, and oil. The reverse micelles characterize the microstructure of the microemulsion and they are able to host solid nanoparticles obtained by in situ reaction and also prevent the agglomeration and precipitation of the nanoparticles which is important for their utilization.

The micelles are aggregates of an amphiphilic molecule called a surfactant; the surfactant molecule lowers the interfacial tension between the solvents and nanoparticles and gives uniform dispersion of particles within the solvent. The solvent also serves a reactor for the synthesis of nanoparticles and the interaction between surfactants and atoms affects the formation of the particle because the binding energies of the ligands affect the growth rate of the different facets and in consequence, the geometry and size of the nanoparticles.

The synthesis of nanoparticles can be done in water containing dioctyl sodium sulfosuccinate (AOT) reverse micelles as nanoreactors [100]. Since the diameter of the aggregates can be varied by changing the molar ratio of water/AOT, then the size of the nanoparticle can be controlled. The synthesis of nanoparticles with uniform size distribution is important for technological applications; in particular, the nanoparticles are used here for the creation of a uniform film on the AFM tip with small roughness since the roughness can drastically affect the measurements of adhesive energy.

The CdS nanoparticles were synthetized according to the methods explained by Tan [101]. In detail, 0.1833 grams of cadmium chloride were dissolved in 50 ml of water to

obtain solution A and 0.24018 grams of sodium sulfide were dissolved in 50 ml water to obtain solution B. AOT was used as surfactant and 0.1677 grams were dissolved in 12.5 ml of hexane to obtain solution C. Solution A and half of C were mixed and then B and half of C, then the two solutions were mixed together. When they were mixed, the reaction took place with immediate color change of the solution. After this, the nanoparticles were separated and remained in a yellow solution. The synthesis of ZnS nanoparticles was similar to the synthesis of CdS nanoparticles but following the methods by Calandra [102], here 0.33 grams of zinc sulfate was used instead of cadmium chloride and 0.2491 grams of sodium sulfide were used. The nanoparticles were separated from the surfactant and they were kept in water for both cases the ZnS and CdS,

The synthesis of the CdSe nanoparticles were carried out differently and it was done according to the methods by Peng and Peng [103]. Here, 0.0514 grams of cadmium oxide (CdO), 2.5 grams of trioctylphosphine oxide (TOPO) and 0.223 grams of tetradecylphosphonic acid (TDPA) were loaded in a three neck flask and the mixture was heated up to 300 °C. Then, the reddish CdO powder was dissolved and generated a colorless homogeneous solution. The introduction of selenium stock solution made with 0.065 grams of selenium powder dissolved in 2 grams of trioctylphosphine (TOP) resulted in the formation of CdSe nanocrystals. This growing mechanism results in high quality nanoparticles and the size of these particles is uniform.

4.3 AFM liftoff test between wurtzite materials and HOPG

The ZnS nanoparticles were used to create a film on the AFM tip; this was done by dipping the AFM tip in the nanoparticle solution and evaporation of the water on the oven at 100 °C. This process was repeated seven times to make sure that a film on the

AFM tip is created. Since the CdS were also kept in water, the same procedure was used to create the CdS film on the AFM tip. For the case of CdSe, first the tip was immersed in methanol, after this step the solution of CdSe nanoparticles solution was dropped into the methanol. Since the CdSe nanoparticles precipitates in methanol, they create and film on the surface of the tip, the tip was removed from the methanol and placed in a convection oven to evaporate the solvent.

After the deposition of the film, the AFM tip was polished with small contact force of 3nN for three minutes, so as to remove any imperfections on the film. It was observed that without this step the adhesive energy was not high since it is highly sensitive to imperfections at the surface; in this case the removal of any surfactants or rough surface by polishing could be the reason for the change of adhesive energy. The film on the tip was removed by hydrochloric acid (HCl) and the adhesive energy of the uncoated tip was tested on HOPG, then the coating procedure was repeated to observe the repeatability of the measurements, as can be observed in Figure 4.1, the values are similar for the uncoated and coated tip. This was done on each set of samples i.e ZnS, CdS and CdSe to make sure the measurements were not influenced by previous coatings.

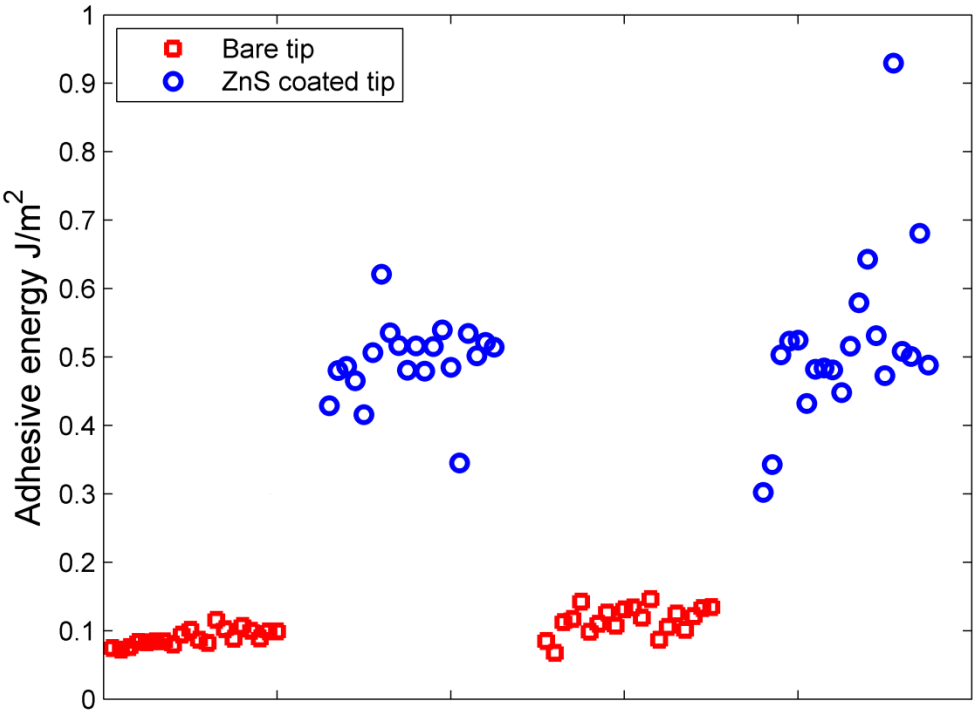

Figure 4.1 Test of adhesive energy between HOPG and ZnS showing the repeatability of the measurement.

The results of the AFM test are shown in Figure 4.2 and they indicate the increase of adhesive energy with ZnS, CdS and CdSe nanoparticles respect to ZnO. The good adhesion of these materials is probably caused by the formation of induced interactions between the ionic material and HOPG. As explained before, this could be because the polar characteristic of these materials creates an induced dipole that interacts with the permanent dipole of the ionic material.

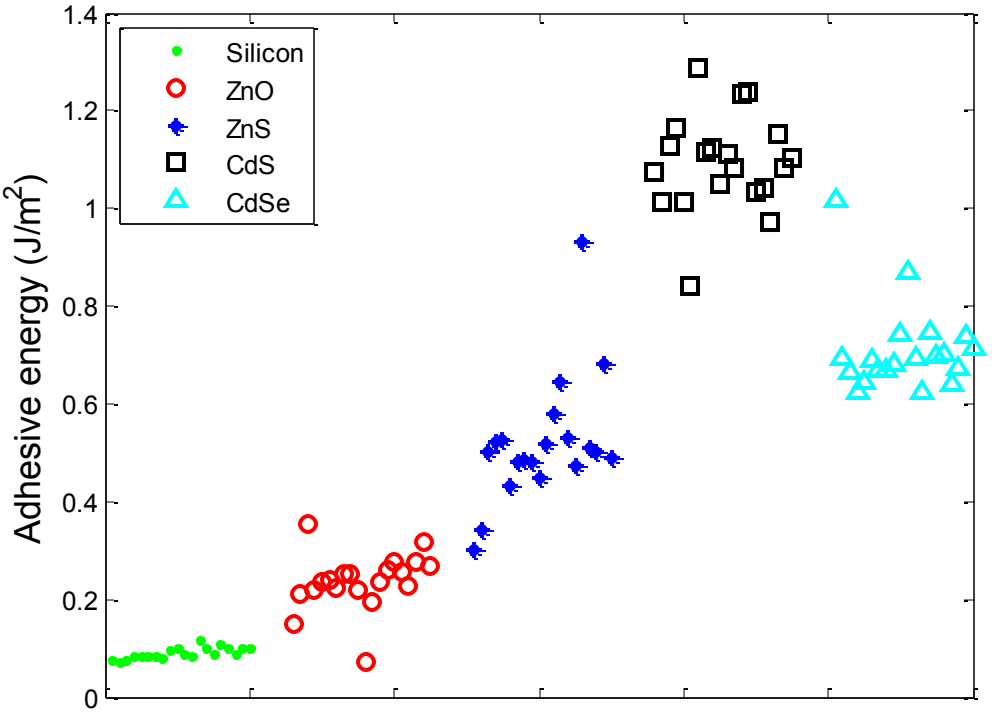

Figure 4.2 Test of adhesive energy of between wurtzite materials and HOPG.

As explained before, the synthesis of the ZnS, CdS and CdSe was performed with the use of micoemulsions. It is possible that surfactant at the surface of the nanoparticles has some influence on the adhesive energy when tested on HOPG. The average adhesive energy of these materials is plotted against the polarizability and this is shown in Figure 4.3. As observed, CdSe has the highest polarizability but it does not show the highest adhesive energy. The highest polarizability of CdSe also means that this is the most unstable material and for this reason, the synthesis of the nanoparticles was different. It is possible that the ligands used for the synthesis affected the adhesive properties of the nanoparticle. As explained before, the surfactants give stability to the nanoparticles, in the case of ZnS and CdS, AOT was used as a surfactant and TOPO was used for the synthesis of CdSe nanoparticles.

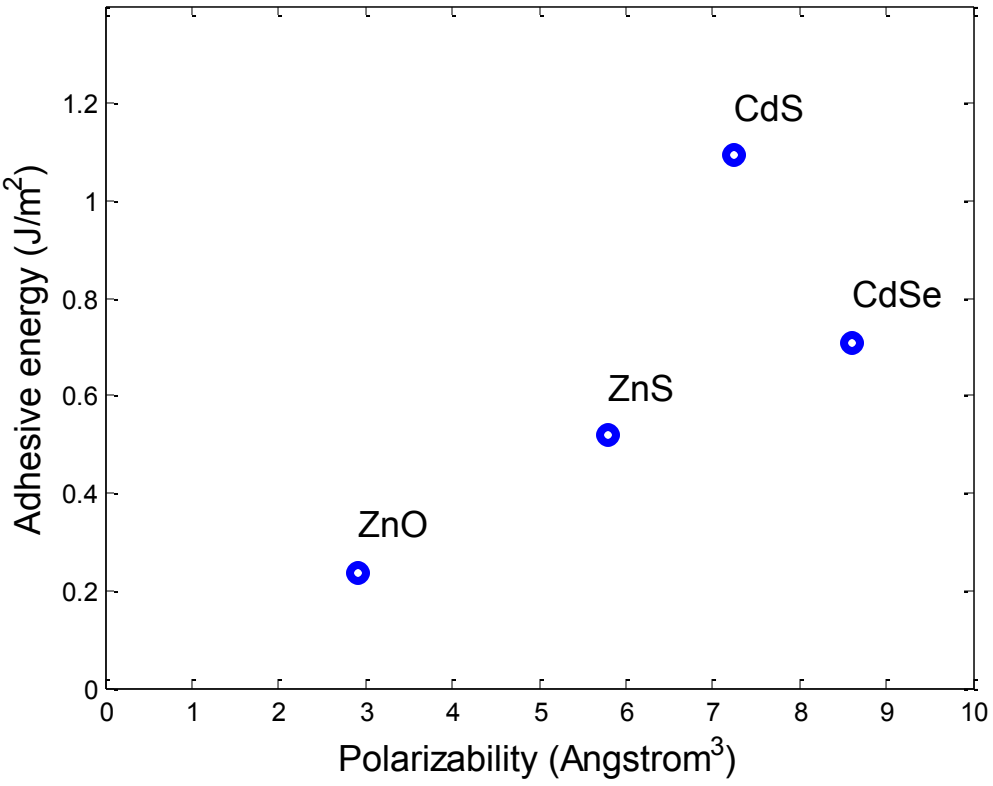

Figure 4.3 Adhesive energy between ZnO, ZnS, CdS and CdSe on HOPG as function of polarizability

4.4 CdS nanoparticles used in carbon fibers

Here two sets of samples are tested and compared: one with CdS film and the other one without the CdS film. Since the CdS nanoparticles have good adhesion to HOPG, these particles were used to create a thin film on the surface of the carbon fiber, then a layer of ZnO was created on top of the CdS nanoparticle film and ZnO nanowires were grown afterwards. These nanowires for the two sets of samples were grown in the same solution to guarantee that the nanowire morphology does not affect the results, but only the nanoparticles attached to the fiber. The procedure to create the film is as follows: the fibers were immersed in the CdS nanoparticle solution, annealed at 150 °C for 10

minutes, and repeated three times. After this step, the ZnO nanoparticles were deposited on the fibers following the same procedure.

ZnO nanowires were grown on the carbon fibers from aqueous solution. For this process, 0.22 grams of zinc nitrate hexahydrate and 0.105 grams of hexamethylenetetramine were dissolved in 500 mL of 18 MΩ-cm Milli-Q water and heated to 90°C under vigorous stirring. Once the solution reached 90 °C, the fibers were immersed in the growth solution for 2.5 hours. After the synthesis, the fibers were rinsed with DI water and a new solution was prepared with the same conditions and the growth was continued for an additional 2.5 hours.

4.5 Single fiber fragmentation test

Single fiber fragmentation samples were prepared by placing a carbon fiber in a dog bond shape mold. The mold was fabricated using silicone (Dow Corning, 3120 RTV Silicone Rubber). The carbon fibers were then carefully suspended on the mold with metal clamps with a mass of 1.15 grams attached to each end of the fiber in order to generate a pre-strain on the fiber. This step is critical to guarantee the saturation of the fiber before failure of the bulk epoxy matrix during the single fiber fragmentation test. The epoxy matrix was prepared by mixing Epon 862 and Epikure 9553 in a 100:16.9 weight ratio. This epoxy was added to the fiber-containing mold and gelled for 2 hours at room temperature. This epoxy matrix is used because it shows good adhesion to bare carbon fiber and fully wets the ZnO nanowires. Moreover, it is optically transparent and tough enough to saturate cracking in fragmentation samples before failure of the polymer matrix. After initial hardening, the samples were removed from the silicone mold and cured in a Fisher Isotemp draft furnace at 100 °C for 1 hour, followed by a post cure at

160 °C for 1 hour. The cured samples were wet polished in order to clearly see the embedded fiber and the cracks formed during testing.

The SFF testing was performed using a linear translation stage with clamps specially designed to fit to the epoxy samples, the displacement was measured with a Linear Variable Displacement Transducer (LVDT) (10mm/V). The samples were mounted in the custom-made fixture and the gauge length for the test was 16 mm. The testing was performed under an optical microscope at 9x magnification, with both polarized and non-polarized light. Non-polarized light allows the viewing of the debonded regions and fiber fracture, while polarized light allows viewing of the birefringence patterns to ensure that only cracks in the fiber due to applied strain are counted. Strain was applied at a rate of 1mm/min and the number of cracks was recorded every 0.7% strain step until saturation was reached.

The method of SFF test [104] to calculate the interfacial shear strength provides qualitative properties of the interface strength. In this test, the load is transmitted from the matrix to fiber and the fiber breaks. Once the fiber breaks, the fiber cannot break within the region in which the stress recovers, furthermore, during the fragmentation of the fiber, there are two types of stresses: the yielding shear stress in the bonded region and the sliding shear stress in the debonding region. In this test, the number of cracks increases until it saturates and the number of cracks denotes the strength between the fiber and matrix. The interfacial shear strength is determined from the Kelly-Tyson equation [105].

$$\tau = \frac{\sigma_f d}{2 l_c} \tag{4.1}$$

where σ_f is the strength of the fiber at the critical length, $\boldsymbol{d}$ is the diameter of the fiber and $\boldsymbol{l_c}$ is the critical length $\boldsymbol{l_c = 4/3l}$, where $\boldsymbol{l}$ is the average segment length.

Thus, the calculation of the shear strength requires knowledge of the fiber strength fiber at the critical length. Tensile strength in small fibers is primarily controlled by the presence of defects through a ”weakest link” behavior and as such, shorter gauge length sections exhibit higher tensile strength than longer gauge sections [106]. Typical critical lengths for single fiber fragmentation testing are in the range of 0.1–1.0 mm; however, these are impractical to test directly. The critical strength of short fibers is typically measured by testing various gauge lengths, fitting the data to a Weibull distribution, and then extrapolating the strength to short fiber lengths. For this analysis, 20 fibers were tested at three gauge lengths and the data was fit using a Weibull distribution. Each set of fibers was fit to a Weibull distribution for both failure stress and failure strain. The confidence intervals are in the 95% confidence limits of the scale parameter of the distribution for both the stress and strain. The tensile strength of the gauge lengths tested were 25.4 mm, 12.7 mm, and 6.35 mm. The scale parameters for the distribution were found to be 5.061 GPa, 5.749 GPa, and 6.176 GPa and the shape parameters were 4.296, 5.918, and 7.067 for the 25.4 mm, 12.7 mm, and 6.35 mm gauge lengths, respectively. The distribution can be extrapolated to shorter gauge lengths once the two parameters (scale and shape) are known. The fitted strengths fall in line with expected values. The fitted shape parameter essentially quantifies the spread or variability in the data due to flaws. Processes that produce additional flaws lead to fibers with high data scatter and a low shape parameter. Typically, carbon fiber exhibits a shape parameter of 5, which is well within the confidence intervals of all estimated shape parameters. These

distributions are then used to predict tensile strength of short gauge lengths in the single fiber fragmentation testing.

The results from the SFF test are shown in Figure 4.4. It can be observed that a higher number of cracks occur in the samples with CdS nanoparticles and this shows the strong interaction between the fiber and the matrix. Thus, the presence of CdS nanoparticles on the surface of the fibers improves the interfacial shear strength compared to the samples that have just a layer of ZnO nanoparticles. These results show that CdS and other ionic materials can be used to improve the mechanical properties of carbon reinforced composites. Furthermore, the results show the importance of the contact area between the carbon fiber surface and the nanoparticles. This interface is critical because the area of the carbon fiber is always the same. This interface is two orders of magnitude smaller than the area of contact between the nanowires and the epoxy matrix, thus, for improvement of the composite interfacial strength it is important to increase the adhesive energy between carbon and the secondary interphase material, which are the CdS nanoparticles in this case. It is interesting to note that even with the small amount of CdS on the surface of the fiber it is enough to increase the strength of the interface. Also, the results suggest that there should be reasonably good bonding between the thin layer of CdS and ZnO so the load can be transmitted to the carbon fiber.

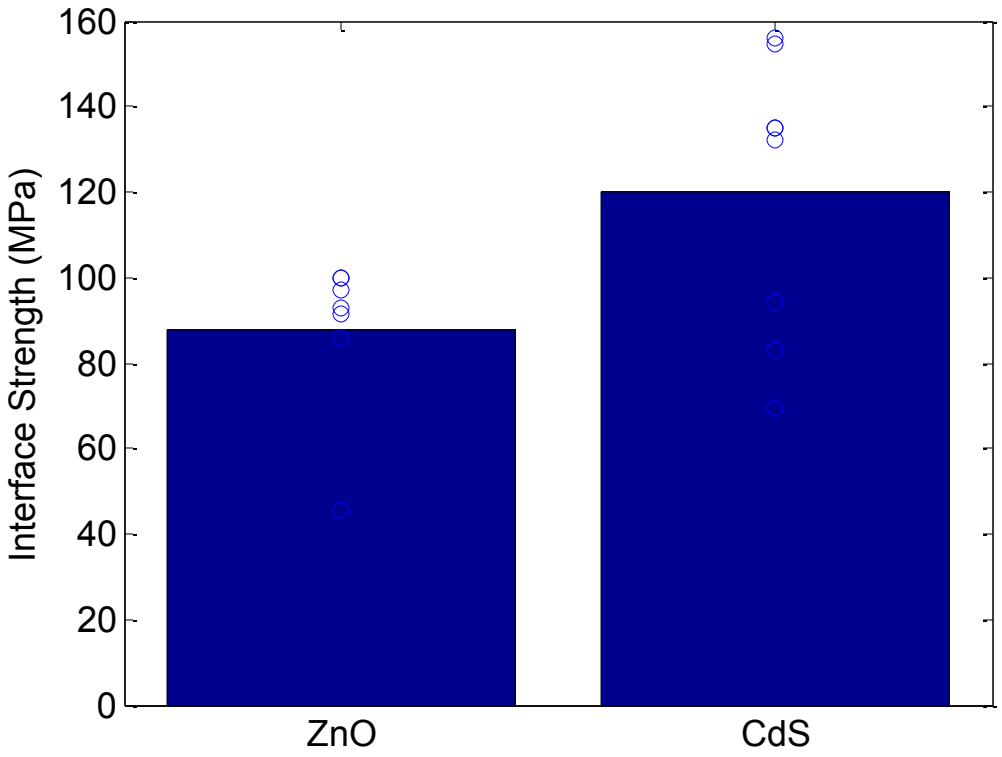

Figure 4.4 Results of SFF test on carbon fibers for ZnO and CdS nanoparticles.

In Figure 4.5, the density of the cracks and the small segments of fiber created by the multiple fractures of the carbon fiber when CdS nanoparticles were annealed on the carbon fiber. Also, during the test, the polymer matrix was fractured more frequently and with more intensity, showing the higher adhesion of the carbon fiber and the matrix. In the case of relative strong interface, the initial crack is followed by a matrix crack; and, in the case of weaker interface, the fiber crack is followed by debonding in the samples without CdS.

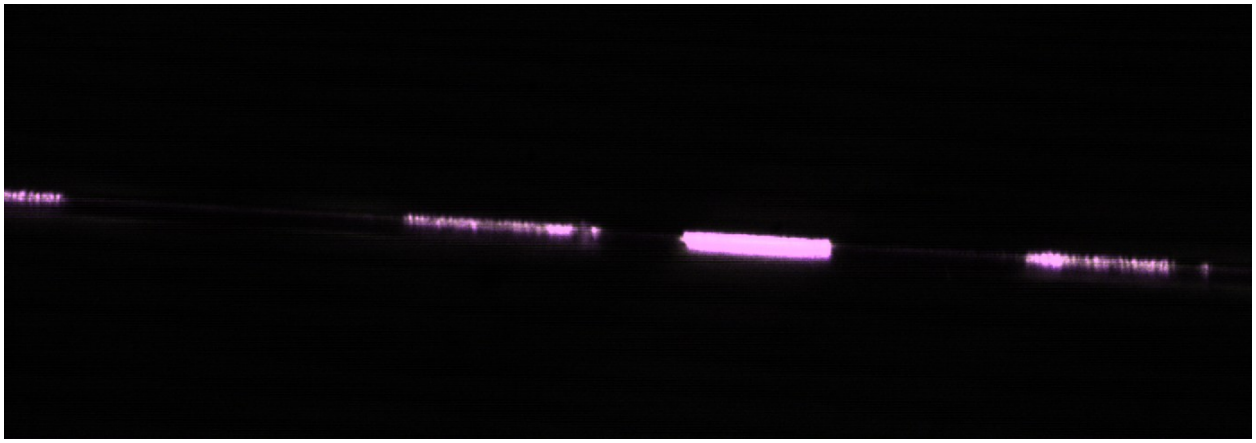

Figure 4.5 Cracks on carbon fiber after single fiber fragmentation test for the CdS nanoparticles samples.

In the AFM liftoff test and the single fiber fragmentation test, CdS resulted in higher strength as compared with ZnO, however the magnitude of the increment was not the same. In the case of the AFM test, the increment was about three times and for the SFF test the increment was 0.5 times. The reason for the relative small increase in the single fiber fragmentation test can be because there are ZnO nanowires grown on the CdS surface; thus, there is an extra CdS/ZnO interface. These materials are similar but the change could affect the strength and this can also be a point of failure. Also, the surface of the fiber is not exactly like the surface of HOPG and the interaction may be different with the functional groups present at the carbon surface.

The results have shown that the ionic materials ZnS, CdS and CdSe have similar properties to ZnO. These materials offer some advantages over ZnO as they shown but also they offer challenges in their application. This is because the synthesis of ZnO is much less complex than other materials and less expensive. Thus, the application of these materials as interphases will be determined by the advances in the methods to scale up the synthesis.

CHAPTER 5

CONCLUSIONS

This dissertation is motivated by the observation of high interfacial shear strength between ZnO nanowires and carbon fibers. This interaction was found to be stronger than the interaction between the epoxy and the fiber, which has been optimized for several decades. In this dissertation the properties of the interface have been studied in order to elucidate the nature of this strong bonding interaction and this chapter shows the conclusions of the research, contributions and suggestion for future work.

5.1 Summary of dissertation and results

In this dissertation a molecular dynamics (MD) model of zinc oxide (ZnO) and carbon has been used to calculate the adhesive energy using intermolecular potentials. Also, functional groups on the carbon surface were simulated and it was observed that ketones showed an increasing adhesive energy with great surface coverage. Unlike hydroxyls and carboxylic acid, the ketones groups showed the capacity to change orientation to increase the interaction with the ZnO surface. Experimentally the atomic force microscope (AFM) was used to calculate the adhesive energy between ZnO and highly oriented pyrolytic graphite (HOPG), the measurements showed good adhesive energy. Then, the HOPG was treated with oxygen plasma to create functional groups, similar to the simulation it was observed an increase of adhesive energy with the increase of oxygen functional groups and it was speculated that the ionic nature of ZnO helped for the increase. The surface of ZnO was modified to hold a negative charge and it was tested on pristine HOPG, which demonstrated an increase in the adhesive energy. This increase in adhesion resulted from the increase in induction forces given that the HOPG

surface is polarized in the presence of the charged ZnO surface and by the fact that the charge on ZnO is not transferred to HOPG since there is an energy barrier [80] associated with the Schottky contact formed between ZnO and HOPG. It was also shown that the increase of polarizability on a silicon substrate resulted in the increase of adhesive energy, since HOPG has a relatively high polarizability it is possible to have strong interactions.

Since it was found that polarizability is important for the induced interactions, other materials with the same ionic characteristics of ZnO but with higher polarizability were studied. It was shown that higher polarizability of the ionic material increases the interaction with carbon, thus, it was concluded that the overall polarizability of the interface is important, not only the polarizability of carbon.

Lastly, cadmium sulfide nanoparticles were used to create a film on the carbon fiber surface and ZnO nanowires were grown on the fibers. From the single fiber fragmentation test, an increase of interfacial shear strength was observed when the CdS nanoparticle film was deposited on the carbon fiber compared to the samples without the CdS nanoparticles, thus, confirming the adhesive properties of CdS nanoparticles on carbon fibers.

5.2 Contributions

MD simulations and AFM liftoff test have been used in this dissertation to study the ZnO-carbon interface; the results of the simulation between ZnO and bare carbon surface showed good agreement with the measurement performed on the AFM. When oxygen functional groups were created on the HOPG surface the adhesive energy increased as measured by the liftoff test. However, in the simulation only the ketones formed strong

interactions with ZnO. This shows that MD models are a useful tool to predict measurements and to give insight about the properties the affect the measurements. In this specific case is not possible to distinguish which functional group contributes more to the increase of adhesive energy when the AFM liftoff test is performed.

Recently, nanostructure materials have been used as interphase to incase the load transfer to carbon fibers in composite materials, and the interface strength has been characterized by testing the bulk composite. Specifically the adhesion of ZnO nanowires to carbon has shown to increase interfacial shear strength and shear modulus of the bulk composites. Given the importance of the solid-solid interface, here the adhesive energy was directly characterized with the use of the AFM. By performing liftoff test in the AFM the intermolecular interactions between ZnO and carbon have been accurately measured. Furthermore, it has been possible to modify the properties of the materials' surface and elucidate the nature of strong intermolecular interactions.

Induction forces were identified by performing liftoff test on different substrates, for the formation of induction forces two conditions are required, a polarizable atomic system and a polar system that distorts the electron cloud of the polarizable system to create a induce dipole that creates an attractive force. In the case of the carbon and ZnO these conditions apply because the relatively high polarizability of carbon and because ZnO is an ionic material with polar surfaces. The magnitude of these forces is significant and can be manipulated by changing the charge on the ZnO surface as shown in chapter 3. Thus, showing that it is faceable to systematically control the adhesive energy at the interface for composite materials.

5.3 Recommendations for future work

5.3.1 Analytical methods

In this dissertation MD simulations were used to calculate the adhesive energy between ZnO and carbon and the interaction between atoms across the interface were modeled with the Lenard Jones potential. Furthermore, all the interactions are represented with a force field plus electrostatic effects that are calculated with the Ewald method. However, these force fields do not necessarily capture the nature of the interactions since the electronic structure of the atoms is not taken into account. In general, the intermolecular interaction can be electrostatic, induction, dispersion, and exchange. The electrostatic interaction occurs between electrically charged systems; the induction interaction is observed when the electronic cloud of an atomic system is distorted by the presence of a dipole; dispersion forces are a weak interaction that occur in nonpolar systems when the adjacent molecules disturb each other electronic cloud; and exchange interactions come from quantum mechanical effects of between identical particles, and these interactions are responsible ferromagnetism among other physical properties of matter.

First principle calculations can be used to calculate the interaction forces at the interface. For example, the symmetry-adapted perturbation theory (SAPT) uses the Density Functional Theory (DFT) approach to calculate electrostatic and induced interactions, thus with this type of calculation it is possible to gain insight about the strength of each of the intermolecular forces. Other Ab initio calculation programs can be used like Vienna Ab initio Simulation Package (VASP) and GAUSSIAN but the calculation of interface strength has to be done according to the Born-Oppenhaimer

approximation $E_{int} = E_{ab} - E_a - E_b$ [107] instead of obtaining the component of each of the interactions (electrostatic, induction, dispersion exchange) like in SAPT. All these types of calculations require high computation power and can be done on a supercomputer or GPU system and the accuracy of the results are not limited by the parameterization of potentials like in the case of MD simulations.

5.3.2 Increase of polarizability on carbon fibers

Ehlert observed that an increase of oxygen on the carbon surface increased the interface strength. Specifically, it was observed that the interface strength was linearly related to the amount of ketones. In MD simulations performed in this dissertation, the presence of ketones on the carbon led to higher adhesive energy but this was not the case of hydroxyls and carboxylic acid. This observation is in agreement with the hypothesis that polarizability can increase the induction interactions, given that ketones have a polarizability of 0.922 $Å^3$ [108], hydroxyls have a polarizability of ~0.0 $Å^3$ [109] and carboxylic acid have polarizability of 0.47 $Å^3$ [110].

Thus, in order to enhance the adhesion of ionic materials and carbon fiber, the polarizability of the functional groups on the carbon fiber can be changed. For example, the ketones present on the carbon fiber can be reacted to obtain thioketones. The thioketone is a molecule is similar to ketone but instead of the oxygen atom there is a sulfur atom. The higher number of electrons of the sulfur atom compared to the oxygen gives the thioketone a larger size and higher polarizability, which is 1.81 $Å^3$ [108] about two times the polarizability of ketones.

The higher polarizability of thioketone also implies that the molecule tends to be more unstable and the synthesis is more difficult. However, some of the functional

groups on carbon fiber can be used to facilitate synthesis. For example, the conversion of C=O into C=S can be done with the use of phosphorus sulfides [111,112]. Also, hydrogen sulfide can react with ketones in a microwave-expedited chemical reaction to obtain thioketones [112]. Alumina encapsulated phosphorus pentasulfide P_4S_{10}/Al_2O_3 has also been used to obtain thioketones in acetonitrile solvent [113].

5.3.3 Use of other polar materials to interface with the carbon fibers

In chapter 4 of this dissertation, the adhesive properties of the ionic materials ZnO, zinc sulfide (ZnS), cadmium sulfide (CdS), and cadmium selenaide (CdSe) were discussed. As explained in chapter 2, the ionic nature of these materials along with the polarizability helped to improve the adhesive energy, thus other materials with ionic nature can be useful as reinforcements. In general, the solid crystals are not completely ionicly or covalently bonded and the degree of each bond is quantified by the bond polarity. Bond polarity measures the degree of inequality in the sharing of electrons between two atoms in a bond. The electronegativity difference between two atoms gives an approximation of the polarity of the bond, the greater the difference, the greater the polarity of the bond, thus, a highly ionic bond has large bond polarity.

Materials with high bond polarity are aluminum nitride (AlN) with bond polarity of 0.808 [114], zinc selenaide (ZnSe) 0.663 [114] and copper bromide (CuBr) 0.819 [114]. AlN nanoparticles can be synthetized by the reaction of hexamethyldisilazane with alumina cupferronate under solvothermal conditions [115]. The synthesis of ZnSe nanoparticles can be done at low temperature with zinc acetate, dimethyl formamide as solvent, thioglycerol as capping agent and sodium selenite as selenium source [116]. CuBr nanoparticles can be synthesized by sonoelectrochemestry of Cu^{2+} ions and

cetyltrimethylammonium bromide, unlike other ionic nanoparticles the CuBr do not require the use of surfactant for the synthesis [117].

5.3.4 Polarity enhancement of nanoparticles.

As shown in chapter 3, the increase on the charge on the surface of ZnO increased the adhesive energy, however the methods used on the AFM to put the charge on the surface of ZnO may not be feasible if the purpose is to have a carbon fiber with ZnO nanowires grown and embedded in a polymer matrix. Nonetheless, it can be interesting to see if the same effect can be obtained by controlling the polarity of the nanoparticles that are used for the creation of the film on the carbon surface.

In chapter 4, ligands were used for the synthesis of nanoparticles because the instability of the nanoparticles can result in undesired size and shape of the nanoparticles, however, the ligands have an extra functionality. For example, organic ligands offer the flexibility of surface modification because the possibilities of incorporating functional groups that can change properties like light sensitivity, hydrophobicity, and polarity. Thus, the polarity of the nanoparticles can be changed with polar ligands such as monosulfonates, trisulfonates, triphenylphosphine; and it has been demonstrated that several different polar and nonpolar ligands can be attached to the nanoparticles. For example the trioctylphosphine oxide ligands that were used for the synthesis of CdSe nanoparticles were replaced with oligoethyleneglycols to allow supramolecular recognition via binding to self-assembled monolayers [118].

REFERENCES

[1] Park SJ. Effect of Fiber–Polymer Interactions on Fracture Toughness Behavior of Carbon Fiber-Reinforced Epoxy Matrix Composites. J Colloid Interface Sci 2000; 228: 287-291.

[2] Nedele MR. Three-dimensional finite element analysis of the stress concentration at a single fibre break. Composites Sci Technol 1994; 51: 517-524.

[3] Tang LG. A review of methods for improving the interfacial adhesion between carbon fiber and polymer matrix. Polymer composites 1997; 18: 100-113.

[4] Thostenson ET. Carbon nanotube/carbon fiber hybrid multiscale composites. J Appl Phys 2002; 91: 6034.

[5] Lin Y. Increased Interface Strength in Carbon Fiber Composites through a ZnO Nanowire Interphase. Advanced functional materials 2009; 19: 2654-2660.

[6] Sager RJ. Effect of carbon nanotubes on the interfacial shear strength of T650 carbon fiber in an epoxy matrix. Composites Sci Technol 2009; 69: 898-904.

[7] Galan U. Effect of ZnO nanowire morphology on the interfacial strength of nanowire coated carbon fibers. Composites Sci Technol 2011.

[8] Százdi L. Electrochemical oxidation of carbon fibres: adsorption of the electrolyte and its effect on interfacial adhesion. Composites.Part A, Applied science and manufacturing 2002; 33: 1361-1365.

[9] Cao H. Uniform modification of carbon fibers surface in 3-D fabrics using intermittent electrochemical treatment. Composites Sci Technol 2005; 65: 1655-1662.

[10] Delamar M. Modification of carbon fiber surfaces by electrochemical reduction of aryl diazonium salts: Application to carbon epoxy composites. Carbon (New York) 1997; 35: 801-807.

[11] Perakslis ED. Surface composition of carbon fibers subjected to oxidation in nitric acid followed by oxygen plasma
. Journal of adhesion science and technology 1997; 11: 531-551.

[12] Wu Z. Nitric acid oxidation of carbon fibers and the effects of subsequent treatment in refluxing aqueous NaOH. Carbon (New York) 1995; 33: 597-605.

[13] Kowbel W. Effect of carbon fabric whiskerization on mechanical properties of C-C composites. Composites Part A, Applied science and manufacturing 1997; 28: 993.

[14] Paipetis A. A study of the stress-transfer characteristics in model composites as a function of material processing, fibre sizing and temperature of the environment. Composites Sci Technol 1997; 57: 827-838.

[15] Paipetis A. Effect of fibre sizing on the stress transfer efficiency in carbon/epoxy model composites. Composites.Part A, Applied science and manufacturing 1996; 27: 755-767.

[16] Fu S-Y. Tensile properties of short-glass-fiber- and short-carbon-fiber-reinforced polypropylene composites. Composites.Part A, Applied science and manufacturing 2000; 31: 1117-1125.

[17] Waltersson K. ESCA studies of carbon fibres: Part III—Surface reactions of carbon fibres with amines. Composites Sci Technol 1985; 23: 303-321.

[18] Xu Z. Influence of rare earth treatment on interfacial properties of carbon fiber/epoxy composites. Materials science & engineering.A, Structural materials : properties, microstructure and processing 2007; 444: 170-177.

[19] Yumitori S. Effect of anodic oxidation of coal tar pitch-based carbon fibre on adhesion in epoxy matrix: Part 2. Comparative study of three alkaline solutions. Composites.Part A, Applied science and manufacturing 1996; 27: 1059-1066.

[20] Park SJ. Studies on PAN-based carbon fibers irradiated by Ar ion beams. J Colloid Interface Sci 2003; 261: 393-398.

[21] Xu Z. Wettability of carbon fibers modified by acrylic acid and interface properties of carbon fiber/epoxy. European polymer journal 2008; 44: 494-503.

[22] Wu GM. Oxygen plasma processing and improved interfacial adhesion in PBO fiber reinforced epoxy composites. Vacuum 2009; 83: S271-S274.

[23] Montes-Morán MA. Effects of plasma oxidation on the surface and interfacial properties of ultra-high modulus carbon fibres. Composites. Part A, Applied science and manufacturing 2001; 32: 361-371.

[24] Yue ZR. Surface characterization of electrochemically oxidized carbon fibers. Carbon (New York) 1999; 37: 1785-1796.

[25] Mader E. Static and dynamic properties of single and multi-fiber/epoxy composites modified by sizings. Composites Sci Technol 2007; 67: 1105-1115.

[26] Dilsiz N. Surface analysis of unsized and sized carbon fibers. Carbon (New York) 1999; 37: 1105-1114.

[27] Yumitori S. The role of sizing resins in carbon fibre-reinforced polyethersulfone (PES). Composites 1994; 25.7: 698-705.

[28] Fu PF. Interposition fixing structure of TiO2 film deposited on activated carbon fibers. Transactions of Nonferrous Metals Society of China 2006; 16: 965-969.

[29] Goan JC. Interfaces in Composites. American Society for Testing and Materials 1969; 1: 3.

[30] Zhang Q. Hierarchical composites of carbon nanotubes on carbon fiber: Influence of growth condition on fiber tensile properties. Composites Sci Technol 2009; 69: 594-601.

[31] Mathur RB. Growth of carbon nanotubes on carbon fibre substrates to produce hybrid/phenolic composites with improved mechanical properties. Composites Sci Technol 2008; 68: 1608-1615.

[32] Garcia EJ. Fabrication and multifunctional properties of a hybrid laminate with aligned carbon nanotubes grown In Situ. Composites Sci Technol 2008; 68: 2034-2041.

[33] Chang PC. ZnO Nanowires Synthesized by Vapor Trapping CVD Method. Chemistry of materials 2004; 16: 5133-5137.

[34] Vayssieres L. Growth of Arrayed Nanorods and Nanowires of ZnO from Aqueous Solutions. Advanced materials (Weinheim) 2003; 15: 464-466.

[35] Tasker PW. The stability of ionic crystal surfaces. Journal of physics.C, Solid state physics 1979; 12: 4977-4984.

[36] Ehlert GJ. Role of Surface Chemistry in Adhesion between ZnO Nanowires and Carbon Fibers in Hybrid Composites. ACS applied materials & interfaces 2013; 5: 635-645.

[37] Purton JA. Comparison of atomistic simulations and pseudopotential calculations of the MgO{100}/Ag{100} and MgO{110}/Ag{110} interfaces. J Chem Phys 1999; 110: 8090.

[38] Hoekstra J. Ab initio calculations of the β-SiC(001)/Al interface. Physical review.B, Condensed matter and materials physics 1998; 57: 2334-2341.

[39] Tanaka S. First-principles study of the adhesive and mechanical properties of the O-terminated -Al O (0001)/Cu(111) interfaces. Philosophical magazine (Abingdon, England) 2006; 86: 5123-5135.

[40] Dandekar CR. Molecular dynamics based cohesive zone law for describing Al-SiC interface mechanics. Composites.Part A, Applied science and manufacturing 2011.

[41] Ryckaert JP. Numerical integration of the cartesian equations of motion of a system with constraints: molecular dynamics of n-alkanes. Journal of computational physics 1977; 23: 327-341.

[42] Rountree CL. Multimillion Atom Molecular Dynamics Simulations. Annual review of materials research 2002; 32: 377-400.

[43] MacElroy JMD. Nonequilibrium molecular dynamics simulation of diffusion and flow in thin microporous membranes. J Chem Phys 1994; 101: 5274.

[44] Falk ML. Dynamics of viscoplastic deformation in amorphous solids. Physical review.E, Statistical physics, plasmas, fluids, and related interdisciplinary topics 1998; 57: 7192-7205.

[45] Nosé S. Constant pressure molecular dynamics for molecular systems. Mol Phys 1983; 50: 1055-1076.

[46] Andersen HC. Molecular dynamics simulations at constant pressure and/or temperature. J Chem Phys 1980; 72: 2384.

[47] Berendsen HJC. Molecular dynamics with coupling to an external bath. J Chem Phys 1984; 81: 3684.

[48] Heiland G. Polar surfaces of zinc oxide crystals. Surf Sci 1969; 13: 72-84.

[49] Dulub O. Novel Stabilization Mechanism on Polar Surfaces: ZnO(0001)-Zn. Phys Rev Lett 2003; 90: 16102.

[50] Lao CS. Formation of double-side teethed nanocombs of ZnO and self-catalysis of Zn-terminated polar surface. Chemical physics letters 2006; 417: 358-362.

[51] Parker EN. Tensor Virial Equations. Physical review 1954; 96: 1686-1689.

[52] Subramaniyan AK. Continuum interpretation of virial stress in molecular simulations. Int J Solids Structures 2008; 45: 4340-4346.

[53] Zhou M. A new look at the atomic level virial stress: on continuum-molecular system equivalence. Proceedings of the Royal Society.A, Mathematical, physical, and engineering sciences 2003; 459: 2347-2392.

[54] Xin Z. Strain energy and Young's modulus of single-wall carbon nanotubes calculated from electronic energy-band theory. Physical review.B, Condensed matter 2000; 62: 13692-13696.

[55] Barone V. Electronic Structure and Stability of Semiconducting Graphene Nanoribbons. Nano letters 2006; 6: 2748-2754.

[56] Eastman T. Adhesion Forces between Surface-Modified AFM Tips and a Mica Surface. Langmuir 1996; 12: 2859-2862.

[57] Florin EL. Adhesion forces between individual ligand-receptor pairs. Science 1994; 264: 415-417.

[58] Carrion-Vazquez M. Mechanical and chemical unfolding of a single protein: A comparison. Proceedings of the National Academy of Sciences - PNAS 1999; 96: 3694-3699.

[59] Liang J. One Bond at a Time. ACS nano 2009; 3: 1628-1645.

[60] Grandbois M. How Strong Is a Covalent Bond? Science (New York, N.Y.) 1999; 283: 1727-1730.

[61] Zhu C. Mechanical Response, Cell Adhesion, and Molecular Deformation. Annu Rev Biomed Eng 2000; 2: 189-226.

[62] Sader JE. Method for the calibration of atomic force microscope cantilevers. Rev Sci Instrum 1995; 66: 3789.

[63] Hu Z. Influence of solvent on the growth of ZnO nanoparticles. J Colloid Interface Sci 2003; 263: 454.

[64] Leftwich TR. Chemical manipulation of multifunctional hydrocarbons on silicon surfaces. Surface science reports 2008; 63: 1.

[65] Horn RG. Contact Electrification and Adhesion Between Dissimilar Materials. Science (New York, N.Y.) 1992; 256: 362-364.

[66] Ehlert GJ. Carboxyl functionalization of carbon fibers through a grafting reaction that preserves fiber tensile strength. Carbon (New York) 2011; 49: 4246-4255.

[67] Jang J. The effect of surface treatment on the performance improvement of carbon fiber/polybenzoxazine composites. J Mater Sci 2000; 35: 2297-2303.

[68] Khlobystov AN. Supramolecular design of one-dimensional coordination polymers based on silver(I) complexes of aromatic nitrogen-donor ligands. Coord Chem Rev 2001; 222: 155-192.

[69] Wang Y. Spectroscopic evidence for the partial dissociation of H2O on ZnO(10$\bar{1}$0). Physical chemistry chemical physics : PCCP 2006; 8: 1521.

[70] Kinbara K. Crystal Structures of the Salts of Chiral Primary Amines with Achiral Carboxylic Acids: Recognition of the Commonly-Occurring Supramolecular Assemblies of Hydrogen-Bond Networks and Their Role in the Formation of Conglomerates. J Am Chem Soc 1996; 118: 3441-3449.

[71] Kochevar IH. Triplet ketone-olefin interactions: energy transfer, charge transfer, or radical addition? J Am Chem Soc 1970; 92: 5742-5743.

[72] Meyer B. Density-functional study of the structure and stability of ZnO surfaces. Physical review.B, Condensed matter 2003; 67: 035403.

[73] Israelachvili J. The hydrophobic interaction is long range, decaying exponentially with distance. Nature (London) 1982; 300: 341-342.

[74] Gou J. Computational and experimental study of interfacial bonding of single-walled nanotube reinforced composites. Computational materials science 2004; 31: 225-236.

[75] Zeng T. Piezoelectric ultrathin polymer films synthesized by electrostatic self-assembly processing. Smart Mater Struct 2000; 9: 801-804.

[76] Bian JM. Synthesis and characterization of two-layer-structured ZnO p-n homojunctions by ultrasonic spray pyrolysis. Appl Phys Lett 2004 ;84: 3783.

[77] Jun JH. Ultraviolet photodetectors based on ZnO nanoparticles. Ceram Int 2009; 35: 2797-2801.

[78] Wang D. The photoluminescence properties of ZnO:N films fabricated by thermally oxidizing Zn N films using plasma-assisted metal-organic chemical vapour deposition. Journal of physics.Condensed matter 2004; 16: 4635-4642.

[79] Lee SY. Fabrication of ZnO thin film diode using laser annealing. Thin Solid Films 2005; 473: 31-34.

[80] Yatskiv R. Semimetal graphite/ZnO Schottky diodes and their use for hydrogen sensing. Carbon (New York) 2012; 50: 3928-3933.

[81] Sivaramakrishnan K. Metallic conductivity and the role of copper in ZnO/Cu/ZnO thin films for flexible electronics. Appl Phys Lett 2009; 94: 052104.

[82] Sahoo S. Self-Assembled Highly Uniform ZnO Submicrometer Rods on Metal Grid Grown by Vapor–Liquid–Solid Method. Crystal growth & design 2011; 11: 3642-3647.

[83] Schmidt MT. Increased dependence of Schottky barrier height on metal work functions due to a thin-oxide layer. Journal of vacuum science & technology.B, Microelectronics processing and phenomena 1988; 6: 1436.

[84] Smith ZE. Intrinsic dangling-bond density in hydrogenated amorphous silicon. Physical review.B, Condensed matter 1985; 32: 5510-5513.

[85] Giessibl FJ. Atomic Resolution of the Silicon (111)-(7x7) Surface by Atomic Force Microscopy. Science (New York, N.Y.) 1995; 267: 68-71.

[86] McCreery RL. Advanced Carbon Electrode Materials for Molecular Electrochemistry. Chem Rev 2008; 108: 2646-2687.

[87] Özgür U. A comprehensive review of ZnO materials and devices. J Appl Phys 2005; 98: 041301.

[88] Xu YN. Electronic, optical, and structural properties of some wurtzite crystals. Physical review.B, Condensed matter 1993; 48: 4335-4351.

[89] Bergstresser TK. Electronic Structure and Optical Properties of Hexagonal CdSe, CdS, and ZnS. Physical review 1967; 164: 1069-1080.

[90] Holt DB. Polarity reversal and symmetry in semiconducting compounds with the sphalerite and wurtzite structures. J Mater Sci 1984; 19: 439-446.

[91] Miura M. Lattice dynamics of wurtzite-type crystals. The Journal of physics and chemistry of solids 1977; 38: 1071.

[92] Iwanaga H. Anisotropic thermal expansion in wurtzite-type crystals. J Mater Sci 2000; 35: 2451-2454.

[93] Ivanov OV. Electronic polarizability of ionic crystals. Solid State Commun 1992; 81: 69-71.

[94] Mahan GD. Polarizability of ions in crystals. Solid State Ionics 1980; 1: 29-45.

[95] Karamanis P. Structure, stability, dipole polarizability and differential polarizability in small gallium arsenide clusters from all-electron ab initio and density-functional-theory calculations. Physical review.A, Atomic, molecular, and optical physics 2008; 77: 013201.

[96] Antoniewicz PR. Surface-Induced Dipole Moments of Adsorbed Atoms. Phys Rev Lett 1974; 32: 1424-1425.

[97] Atay T. Strongly Interacting Plasmon Nanoparticle Pairs: From Dipole−Dipole Interaction to Conductively Coupled Regime. Nano letters 2004; 4: 1627-1631.

[98] Xue BK. Growth of Pd, Pt, Ag and Au nanoparticles on carbon nanotubes. Journal of materials chemistry 2001; 11: 2378-2381.

[99] Capek I. Preparation of metal nanoparticles in water-in-oil (w/o) microemulsions. Adv Colloid Interface Sci 2004; 110: 49-74.

[100] Kim DW. Preparation of Ultrafine Monodispersed Indium−Tin Oxide Particles in AOT-Based Reverse Microemulsions as Nanoreactors. Langmuir 1999; 15: 1599-1603.

[101] Tan L. Fluorescence Quenching of Bovine Serum Albumin in Reversed Micelles by CdS Nanoparticles. Analytical sciences 2004; 20: 441-444.

[102] Calandra P. Study of the growth of ZnS nanoparticles in water/AOT/n-heptane microemulsions by UV-absorption spectroscopy. Colloids and surfaces.A, Physicochemical and engineering aspects 1999; 160: 9-13.

[103] Peng ZA. Formation of high-quality CdTe, CdSe, and CdS nanocrystals using CdO as precursor. J Am Chem Soc 2001; 123: 183-184.

[104] Varna J. Interfacial toughness evaluation from the single-fiber fragmentation test. Composites Sci Technol 1996; 56: 1105-1109.

[105] Kelly A. Tensile properties of fibre-reinforced metals: copper/tungsten and copper/molybdenum. J Mech Phys Solids 1965; 13: 329.

[106] Padgett WJ. Weibull Analysis of the Strength of Carbon Fibers Using Linear and Power Law Models for the Length Effect. J Composite Mater 1995; 29: 1873-1884.

[107] Pisana S. Breakdown of the adiabatic Born–Oppenheimer approximation in graphene. Nature materials 2007; 6: 198-201.

[108] Miller KJ. Additivity methods in molecular polarizability. J Am Chem Soc 1990; 112: 8533-8542.

[109] Anisimov VM. Polarizable Empirical Force Field for the Primary and Secondary Alcohol Series Based on the Classical Drude Model. Journal of chemical theory and computation 2007; 3: 1927-1946.

[110] Ohno H. Amino Acid Ionic Liquids. Acc Chem Res 2007; 40: 1122-1129.

[111] Mayer R. Aliphatic Thioketones. Angewandte Chemie (International ed.) 1964; 3: 277-286.

[112] Varma RS. Microwave-Accelerated Solvent-Free Synthesis of Thioketones, Thiolactones, Thioamides, Thionoesters, and Thioflavonoids. Org Lett 1999; 1: 697-700.

[113] Polshettiwar V. A new, efficient and simple method for the thionation of ketones to thioketones using P4S10/Al2O3. Tetrahedron Lett 2004; 45: 6255-6257.

[114] Lambrecht WRL. Interface-bond-polarity model for semiconductor heterojunction band offsets. Physical review.B, Condensed matter 1990; 41: 2832-2848.

[115] Sardar K. AlN nanocrystals by new chemical routes. Solid state sciences 2005; 7: 217-220.

[116] Deshpande AC. Low temperature synthesis of ZnSe nanoparticles. Mater Lett 2008; 62: 3803-3805.

[117] Haas I. Sonoelectrochemistry of Cu in the Presence of Cetyltrimethylammonium Bromide: Obtaining CuBr Instead of Copper. Chemistry of materials 2006; 18: 1184-1189.

[118] Binder WH. Surface-modified nanoparticles via thermal and Cu(i)-mediated click chemistry: Generation of luminescent CdSe nanoparticles with polar ligands guiding supramolecular recognition. Journal of materials chemistry 2007; 17: 2125